Atmospheric
Chemistry
and Physics
Discussions

Open Access

A comprehensive laboratory study on the immersion freezing behavior of illite NX particles: a comparison of seventeen ice nucleation measurement techniques
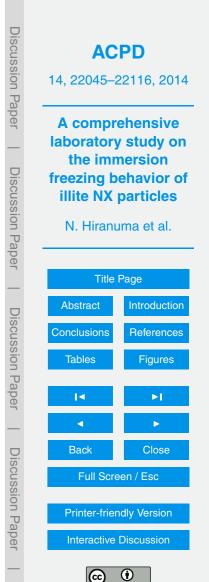
N. Hiranuma[1], S. Augustin-Bauditz[2], H. Bingemer[3], C. Budke[4], J. Curtius[3],
A. Danielczok[3], K. Diehl[5], K. Dreischmeier[4], M. Ebert[6], F. Frank[3], N. Hoffmann[1],
K. Kandler[6], A. Kiselev[1], T. Koop[4], T. Leisner[1], O. Möhler[1], B. Nillius[3,*],
A. Peckhaus[1], D. Rose[3], S. Weinbruch[6], H. Wex[2], Y. Boose[7], P. J. DeMott[8],
J. D. Hader[9], T. C. J. Hill[8], Z. A. Kanji[7], G. Kulkarni[10], E. J. T. Levin[8],
C. S. McCluskey[8], M. Murakami[11], B. J. Murray[12], D. Niedermeier[2,**],
M. D. Petters[9], D. O'Sullivan[12], A. Saito[11], G. P. Schill[13], T. Tajiri[11],
M. A. Tolbert[13], A. Welti[7], T. F. Whale[12], T. P. Wright[9], and K. Yamashita[11,***]

[1]Institute for Meteorology and Climate Research – Atmospheric Aerosol Research, Karlsruhe Institute of Technology, Karlsruhe, Germany
[2]Leibniz Institute for Tropospheric Research, Leipzig, Germany
[3]Institute for Atmospheric Physics, University of Mainz, Mainz, Germany
[4]Faculty of Chemistry, Bielefeld University, Bielefeld, Germany

Title Page

Abstract	Introduction
Conclusions	References
Tables	Figures

|◄ | ►|
◄ | ►
Back | Close

Full Screen / Esc

Printer-friendly Version

Interactive Discussion

[5]Institute for Atmospheric and Environmental Science, Goethe University of Frankfurt, Frankfurt, Germany
[6]Institute of Applied Geosciences, Technical University Darmstadt, Germany
[7]Institute for Atmosphere and Climate Science, ETH, Zurich, Switzerland
[8]Department of Atmospheric Science, Colorado State University, Fort Collins, CO, USA
[9]Department of Marine Earth and Atmospheric Sciences, North Carolina State University, Raleigh, NC, USA
[10]Atmospheric Science and Global Change Division, Pacific Northwest National Laboratory, Richland, WA, USA
[11]Meteorological Research Institute (MRI), Tsukuba, Japan
[12]Institute for Climate and Atmospheric Science, School of Earth and Environment, University of Leeds, Leeds, UK
[13]Cooperative Institute for Research in Environmental Sciences and Department of Chemistry and Biochemistry, University of Colorado, Boulder, CO, USA
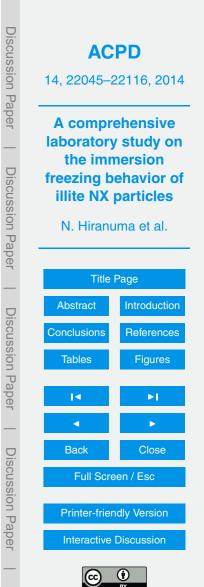[*]Max-Planck-Institut für Chemie, Mainz, Germany
[**]Department of Physics, Michigan Technological University, Houghton, MI, USA
[***]Snow and Ice Research Center, Nagaoka, Japan

Correspondence to: N. Hiranuma (seong.moon@kit.edu)

Title Page

Abstract | Introduction

Conclusions | References

Tables | Figures

|◄ | ►|

◄ | ►

Back | Close

Full Screen / Esc

Printer-friendly Version

Interactive Discussion

Abstract

Immersion freezing is the most relevant heterogeneous ice nucleation mechanism through which ice crystals are formed in mixed-phase clouds. In recent years, an increasing number of labora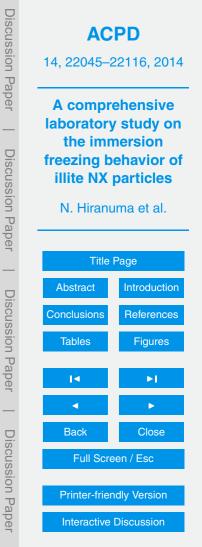tory experiments utilizing a variety of instruments have examined immersion freezing activity of atmospherically relevant ice nucleating particles (INPs). However, an inter-comparison of these laboratory results is a difficult task because investigators have used different ice nucleation (IN) measurement methods to produce these results. A remaining challenge is to explore the sensitivity and accuracy of these techniques and to understand how the IN results are potentially influenced or biased by experimental parameters associated with these techniques.

Within the framework of INUIT (Ice Nucleation research UnIT), we distributed an illite rich sample (illite NX) as a representative surrogate for atmospheric mineral dust particles to investigators to perform immersion freezing experiments using different IN measurement methods and to obtain IN data as a function of particle concentration, temperature (T), cooling rate and nucleation time. Seventeen measurement methods were involved in the data inter-comparison. Experiments with seven instruments started with the test sample pre-suspended in water before cooling, while ten other instruments employed water vapor condensation onto dry-dispersed particles followed by immersion freezing. The resulting comprehensive immersion freezing dataset was evaluated using the ice nucleation active surface-site density (n_s) to develop a representative $n_s(T)$ spectrum that spans a wide temperature range ($-37\,^\circ\text{C} < T < -11\,^\circ\text{C}$) and covers nine orders of magnitude in n_s.

Our inter-comparison results revealed a discrepancy between suspension and dry-dispersed particle measurements for this mineral dust. While the agr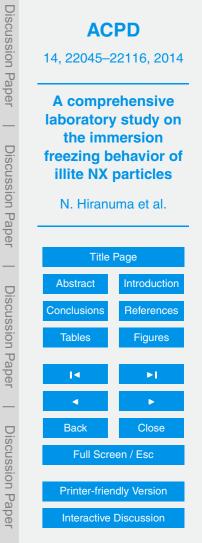eement was good below $\sim -26\,^\circ\text{C}$, the ice nucleation activity, expressed in n_s, was smaller for the wet suspended samples and higher for the dry-dispersed aerosol samples between about -26 and $-18\,^\circ\text{C}$. Only instruments making measurement techniques with wet suspended samples were able to measure ice nucleation above $-18\,^\circ\text{C}$. A possible explanation

for the deviation between -26 and $-18\,^\circ$C is discussed. In general, the seventeen immersion freezing measurement techniques deviate, within the range of about $7\,^\circ$C in terms of temperature, by three orders of magnitude with respect to n_s. In addition, we show evidence that the immersion freezing efficiency (i.e., n_s) of illite NX parti-cles is relatively independent on droplet size, particle mass in suspension, particle size and cooling rate during freezing. A strong temperature-dependence and weak time- and size-dependence of immersion freezing efficiency of illite-rich clay mineral particles enabled the n_s parameterization solely as a function of temperature. We also characterized the $n_s(T)$ spectra, and identified a section with a steep slope be-tween -20 and $-27\,^\circ$C, where a large fraction of active sites of our test dust may trigger immersion freezing. This slope was followed by a region with a gentler slope at temperatures below $-27\,^\circ$C. A multiple exponential distribution fit is expressed as $n_s(T) = \exp(23.82 \times \exp(-\exp(0.16 \times (T + 17.49))) + 1.39)$ based on the specific sur-face area and $n_s(T) = \exp(25.75 \times \exp(-\exp(0.13 \times (T + 17.17))) + 3.34)$ based on the geometric area (n_s and T in m^{-2} and $^\circ$C, respectively). These new fits, constrained by using an identical reference samples, will help to compare IN measurement methods that are not included in the present study and, thereby, IN data from future IN instru-ments.

1 Introduction

Primary ice formation by atmospheric ice nucleating particles (INPs) markedly influ-ences the formation and life cycle of mixed-phase clouds and very often also initiates precipitation formation. Therefore, ice-containing clouds play a significant role in the energy balance of the climate system and the hydrological cycle on Earth (Chapter 7 of IPCC, 2013; Boucher et al., 2013). Currently, quantitative predictions for the im-pact of these clouds on the Earth's radiative budget and thereby the climate are highly uncertain. This uncertainty arises primarily from a lack of fundamental understanding of ice microphysical processes, the representation of these processes in cloud mod-

Title Page

Abstract | Introduction

Conclusions | References

Tables | Figures

|◄ | ►|

◄ | ►

Back | Close

Full Screen / Esc

Printer-friendly Version

Interactive Discussion

els and knowledge of the abundance of INPs (Hoose and Möhler, 2012; Murray et al., 2012).
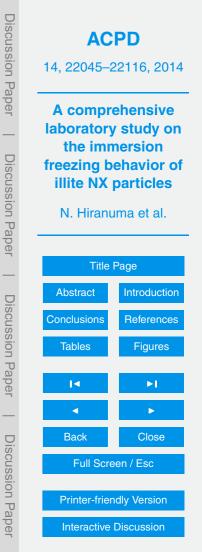
A small subset of all particles acts as INPs across a range of subzero temperatures, triggering ice formation in clouds via the process of heterogeneous ice nucleation. Previous laboratory experiments have taken diverse approaches in an attempt to mimic ice nucleation and freezing processes. These heterogeneous ice formation processes include deposition nucleation, immersion-, condensation- and contact freezing (Vali, 1985), inside-out contact freezing (i.e., freezing of an immersed INP contacting the droplet surface from the inside; Durant and Shaw, 2005; Fornea et al., 2009) and surface condensation freezing (i.e., freezing of supercooled water or residual aqueous solution trapped on particle surfaces, e.g., by the inverse Kelvin effect; Christenson, 2013; Hiranuma et al., 2014a; Marcolli, 2014; Welti et al., 2014; Wex et al., 2014). Without INPs, pure cloud water droplets or solution within particles can supercool to below $-37\,°C$ and initiate freezing (Koop et al., 2000; Murray et al., 2010; Rosenfeld and Woodley, 2000).

Among the various modes of atmospheric ice nucleation, immersion freezing is one of the most important mechanisms for primary ice formation in 85 % of ice formation in clouds that contain supercooled droplets (Hoose et al., 2010). Furthermore, many of the previous experimental studies have investigated heterogeneous ice nucleation at conditions where water is supercooled before freezing (e.g., Murray et al., 2012). However, the relative importance of the particles' physico-chemical properties (i.e., size, composition, solubility, hygroscopicity, cloud condensation nuclei activity, ice nucleation (IN) active sites, surface charge and/or crystallographic structure) towards immersion freezing properties is not yet well known (e.g., Hiranuma et al., 2013, 2014b; Murray et al., 2012). Hence, more in-depth investigations and understanding of heterogeneous ice nucleation processes in mixed-phase clouds, where supercooled liquid water and ice coexist, is of particular importance.

The concept of condensation nuclei contributing to ice formation was first introduced by Alfred Wegener in 1911 (Wegener, 1911). Afterwards, various instruments
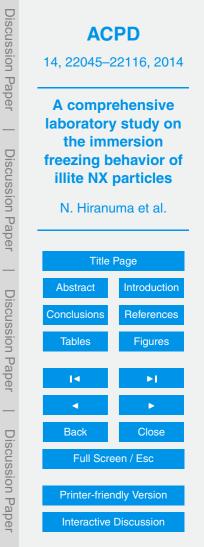
and methods have been developed to investigate the composition of atmospherically relevant INPs as well as their abundance; for example, the rapid expansion cloud-simulation chamber (RECC), which was first introduced as a detector of ionizing particles. Such instruments have been used in many ice nucleation studies since the 1940s

⁵ (e.g., Cwilong, 1947; Fournier d'Albe, 1949; Palmer, 1949; Bigg, 1957; Kline and Brier, 1961). Supersaturated conditions both with respect to water and ice, as a function of temperature, in the simulation chamber vessel were realized by a rapid pressure drop caused by mechanical expansion and subsequent cooling. Water vapor in the supersaturated air can either deposit or condense on sample particles, leading to the formation

¹⁰ of water droplets and/or ice.

A different type of instrument widely used to measure abundance and efficiency of INPs is the continuous flow diffusion chamber (CFDC). The need for portable instruments capable of obtaining continuous measurements for aircraft applications emerged in discussions during the 1970s and was a main driver of CFDC development. In

¹⁵ CFDCs, particles are sampled into a region between two ice-coated concentric cylinders (or dual parallel plates) maintained at different temperatures, which generates a region of ice supersaturation between ice-coated walls. As the particles experience ice supersaturation conditions for a few seconds, INPs can be activated and diffusively grow to supermicron ice crystals. Typically, these large ice crystals can be detected and

²⁰ counted by an optical particle counter (OPC) downstream of the instrument while the chamber temperature and humidity conditions are continuously recorded. Since its first appearance in the 1980s with horizontal parallel plates (Hussain and Saunders, 1984; Tomlinson and Fukuta, 1985), several new designs and operational principles were introduced (e.g., vertically oriented cylinders; Rogers et al., 1988, horizontally oriented

²⁵ parallel plates; Kanji and Abbatt, 2009, vertically oriented parallel plates; Stetzer et al., 2008; Chou et al., 2011; Friedman et al., 2011). An alternative configuration is the continuous flow mixing chamber (e.g., Fast Ice Nucleus Chamber or FINCH; Bundke et al., 2008). The operation principle of this type of chamber does not involve water vapor diffusion from the ice walls, as like in CFDC, but water vapor is available for ice growth
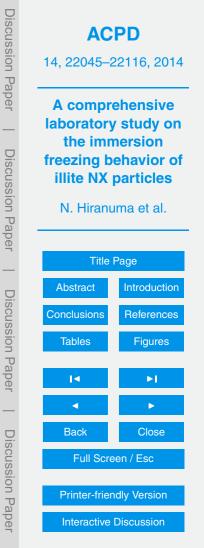
from the humidified air available within the chamber flow. This leads to an upper limit on INP concentrations that are observable with this methodology (DeMott et al., 2011). Furthermore, a flow tube (e.g., Leipzig Aerosol Cloud Interaction Simulator or LACIS, Hartmann et al., 2011) has been developed in which a humidified stream containing aerosol particles is first cooled to activate droplets on the particles, which upon further cooling may then freeze.

In addition to chamber techniques, the mode-specific conditions for heterogeneous ice nucleation of a known INP placed on a substrate surface has been studied using optical microscope techniques. For example, by collecting a series of images at controlled cooling rates, the change in reflectivity and opacity during ice formation can be characterized, and the associated freezing conditions of ice nuclei immersed in water droplets placed on a hydrophobic substrate surface can also be identified (e.g., Knopf and Alpert, 2013; Murray et al., 2011). More recently, other optical microscopy techniques coupled with a unique method of encapsulating particles into droplet followed by cooling (Iannone et al., 2011) or using the hydrophobic squalene/water emulsion (Wright and Petters, 2013) were introduced to the community. Using a similar approach, substrate-supported cooling studies have been applied to determine the freezing temperature in the contact mode (e.g., Fornea et al., 2009; Niehaus et al., 2014), or of deposition nucleation (e.g., Kanji and Abbatt, 2006; Bingemer et al., 2012; Dymarska et al., 2006). The microscopy-coupled substrate-supported freezing devices are advantageous to visualize the consequences of specific ice nucleation modes in controlled and simulated environments. In some studies, immersion freezing of μL scale droplet volumes were analyzed at temperatures (T_s) higher than −10 °C with a sensitivity of INP concentration as good as $\sim 10^{-5}\,\mathrm{L}^{-1}$ (Ardon-Dreyer et al., 2011).

The freezing temperature of INPs either immersed in or in contact with levitated supercooled water droplets suspended in the air can also be determined by the change in light scattering with a charge-coupled device (CCD) camera using an electrodynamic balance (EDB; Hoffmann et al., 2013), an acoustic levitator (Diehl et al., 2014) or in a vertical wind tunnel (Szakáll et al., 2009). The advantage of these methods is the
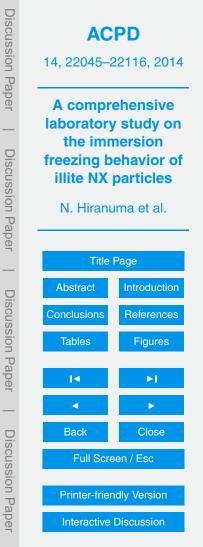
ability to provide, via high-resolution images, substrate-free information for statistically representative ice nucleation processes on a single droplet basis. This advantage is shared with all of the above mentioned chamber and flow tube devices.

Undoubtedly, these enormous efforts to develop numerous IN measurement techniques have advanced our basic knowledge of atmospheric ice formation. As a consequence, the atmospheric science community will continue to pursue investigations of IN to unravel their associated effects on climate. Accordingly, exploring the sensitivities, uncertainties and biases of various experimental techniques (e.g., methods for particle generation, size segregation, size estimation, ice detection and any other notable experimental procedures) in nucleating ice on particles of known physico-chemical properties is crucial in order to compile comparative INP data of multiple and complex measurement techniques from various research institutions. The information obtained from one technique guides other measurement techniques (DeMott et al., 2011; Riechers et al., 2013). A better understanding of the sensitivity of multiple techniques and the role of associated experimental parameters upon INP measurements will also help in transferring the laboratory-based measurements of INPs of various atmospheric constituents to their reliable parameterization in models of atmospheric processes.

Since the 1960s, four international workshops have been organized to compare the performance of IN measuring instruments that were emerging or available at the time (DeMott et al., 2011). In particular, effort was made during the fourth international ice nucleation workshop in 2007 (ICIS-2007) to assemble a total of nine laboratory and field IN instruments at the AIDA facility and compare them using identical test dust samples (e.g., Arizona Test Dust or ATD and Saharan Dust) over similar thermodynamic conditions. State-of-the-art knowledge was obtained from each workshop activity, and such measurement understanding was further incorporated to develop next generation of IN instruments.

The major aim of this study, and concurrent studies within the framework of the INUIT (Ice Nucleation research UnIT) project, was to investigate the immersion freezing behavior of reference particles (e.g., Snomax for bacterial IN processes and potassium-
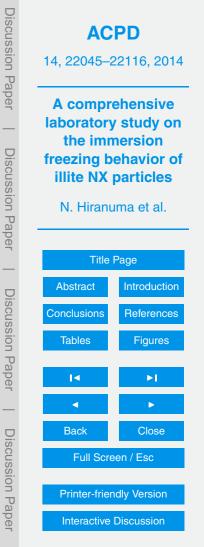
rich feldspar, K-feldspar, as mineral dust). In this work, we distributed illite NX samples from the same batch (with the exceptions of the samples used for Leeds-NIPI, ZINC and IMCA-ZINC; Broadley et al., 2012; Welti et al., 2009) among the INUIT project and associated partners. With a total of seventeen different IN measuring instruments, we inter-compared IN data from each instrument in order to get a comprehensive dataset for evaluating immersion freezing properties of illite NX particles. The dataset consti- tutes a function of various experimental parameter variables such as particle concen- tration, particle size, droplet size, temperature, cooling rate and nucleation time. Fur- ther, some instruments used test samples suspended in water prior to experiments, while others used dry-dispersed particles. The basic experimental methods and pa- rameterization approaches used to interpret the overall results and perform the inter- comparison are discussed.

Results of freezing efficiencies at specific temperatures are presented using the ice nucleation active surface-site density (n_s) parameterization (e.g., Connolly et al., 2009; Niemand et al., 2012; Hoose and Möhler, 2012). For instance, Niemand et al. (2012) showed that the singular parameterization-approach of immersion freezing (i.e., freez- ing along water saturation conditions while cooling) of various desert dust particles derived from AIDA experiments converge upon one representative fit as a function of temperature, which is valid across a temperature range from −12 to −36 °C. The time-independent n_s parameterization has also been demonstrated for describing INP activation by several different constituents of clay minerals, e.g., microcline and kaoli- nite, using the cold stage droplet freezing technique (Atkinson et al., 2013; Murray et al., 2011; Murray et al., 2010). Hence, comparison of the IN efficiencies can be readily performed for multiple types of instruments using n_s parameterizations. Moreover, such time-independent and surface-area-scaled n_s formulations can be further adapted to comprehensively assess ice nucleation in a wide range of atmospherically relevant temperatures and relative humidities with respect to ice (RH_{ice}), as was recently pre- sented in Hiranuma et al. (2014a). The n_s parameterization for both immersion freezing and deposition nucleation can be directly implemented in cloud, weather and climate
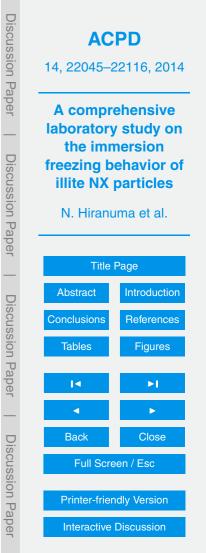
models to calculate the temperature-dependent abundance of INPs as a function of the aerosol surface area concentration.

2 Methods

2.1 Illite NX characterization

Yearly emission rates of soil dust are 1000 to 4000 teragrams, accounting for a major proportion of both the dust component and the total particle loading in the atmosphere. The resulting radiative forcing directly exerted by mineral dust is estimated to range from -0.3 to $+0.1\,\mathrm{W\,m^{-2}}$; therefore, dust slightly contributes to the direct cooling effect of aerosols (Boucher et al., 2013). However, our understanding of the influence of the dust burden upon overall climate forcing and the consequent cloud albedo effect remains highly uncertain, in part due to the absence of accurate INP representations in atmospheric models. Thus, the indirect radiative forcing effect of dust on current climate predictions remains unresolved. In this study, we have chosen illite NX (Arginotec, NX Nanopowder) as a surrogate for natural desert dusts. This choice of an illite rich material is based on a comparison of its mineralogical composition to that of desert dusts, which are also rich in illite but are also mixed with a range of other minerals (Broadley et al., 2012). The present work gives an overview of laboratory experiments for immersion freezing of particles of illite NX, used as a surrogate for atmospheric desert dust particles. Illite NX bulk powder was previously characterized for its physico-chemical properties, such as mineralogy and specific surface area (SSA or θ for brevity). It was observed that illite NX samples contained more than 74 weight percent (wt%) illite (Broadley et al., 2012; Friedrich et al., 2008) along with other components [kaolinite, quartz, calcite and feldspars (most likely orthoclase/sanidine), see Sect. 3.1 for more detail] which is similar to the X-ray diffraction (XRD) data specified by the manufacturer. These test particles had aggregates of many nanometer-sized grains, yielding an order of magnitude greater SSA ($104.2\,\mathrm{m^2\,g^{-1}}$; Broadley et al., 2012). The aspher-

ical and elongated nature of illite NX particles (aspect ratio up to ~ 4.8; Veghte and Freedman, 2014) emphasizes the importance of considering its deformed shape. The manufacturer reports the particle density, after mechanical granulation, as $2.65\,g\,cm^{-3}$.
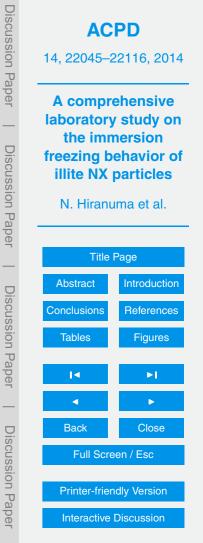
To determine the purity of our sample, and to compare this with previous observations, the dust mineralogy of a bulk illite NX sample was characterized using XRD (Waseda et al., 2011) prior to distribution. In addition, complementary energy dispersive X-ray (EDX) spectroscopy analysis was performed to characterize the elemental composition of individual particles. The illite NX particles were sampled directly from the AIDA chamber using a 47 mm Nuclepore® filter (Whatman, 0.2 μm pore-size, filter Cat. No. 111106) and used in the EDX analysis.

The N_2-adsorption-based SSA (or BET surface, Brunauer, Emmett, and Teller, 1938) of the illite NX sample was also measured. BET is a gas adsorption technique where the quantity of various gases required to form a monolayer over the entire available surface of dry particles, including internal surfaces, is measured (Gregg and Sing, 1982; Bickmore et al., 2002). From the knowledge of the size of a molecule on the surface, it is possible to determine the total surface area (S_{total}). In this work, BET surface areas were determined using two different gas adsorbents: N_2 and H_2O (resulting in θ_{N_2} and θ_{H_2O}), with the latter being the effective surface area exposed to water. BET measurements with H_2O were limited to 28 % relative humidity with respect to water (RH_w) to correctly account for a monolayer of H_2O (Quantachrome Instruments, 2013).

The effect of particle processing, such as removal of hydrophilic ions by water, in a water suspension was examined by ion chromatography (IC). The influence of dust washing and discharge of soluble materials on IN propensity has been previously reported (Welti et al., 2014). Suspended samples were prepared by stirring illite NX powders (0.1 g in 10 mL of 18.2 MΩ nanopure water) over three weeks. IC (Dionex DX–500 IC System equipped with Dionex CD20 Conductivity Detector) was used to determine the concentrations of washed out cations (K^+, Na^+, Ca^{2+}, Mg^{2+}) as a function of time. A weak solution of sulfuric acid (5mL H_2SO_4 (96 wt %) diluted in 2 L of Nanopure water) was used as the eluent. The measurements were conducted in three series: every 5
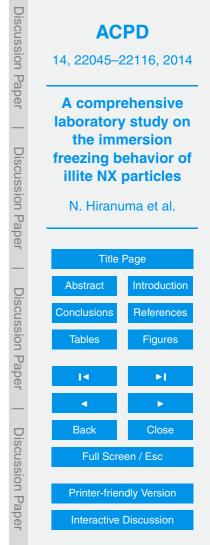
to 10 s (seconds) within the first 2 min (minutes) (ultra short time series, USTS), then every 10 min within the first hour after immersion (short time series, STS) followed by a long time series (LTS) with cation concentration measurements conducted every 2 days thereafter for a three week period.

2.2 Particle size distribution

Size distributions and the S_{total} (in $m^2\,cm^{-3}$) of both suspended and dry-dispersed illite NX particles were characterized using four size measurement techniques (i.e., aerosol size spectrometers and light scattering instruments). In particular, the dynamic light scattering (DLS) size of suspended illite NX particles (0.05 to 1 mg bulk illite NX sample in 1 mL of triple-distilled water) was determined using the StabiSizer® (Microtrac Europe GmbH, PMX 200CS) over the range of 0.0008 to 6.5 µm hydrodynamic diameter. A more detailed description of this instrument and its application for studying the size of particles in suspension are addressed in Hiranuma et al. (2014b), and only a brief discussion is given here. The DLS measurements were carried out with negligible contribution of multiple scattering due to the utilized 180° backscattering mode. The hydrodynamic diameter, which is comparable to the volume equivalent diameter, is determined using a refractive index of 1.55 to 1.58 for illite and of 1.333 for water, and a viscosity of water of 1.002 mPa s and 0.797 mPa s at 20 and 30 °C, respectively. From this metric, the surface area is calculated assuming spherical particles.

Size distributions of dry polydisperse illite NX particles were measured at AIDA controlled expansion cloud-simulation chamber (CECC) and MRI dynamic CECC (DCECC, acronyms are defined in the Supplementary Information) prior to the expansion experiments. For AIDA-CECC, de-agglomerated illite NX particles from a rotating brush disperser (PALAS, RGB 1000) were passed through a series of inertial cyclone impactor stages ($D_{50} \sim 1$ and 5 µm) and introduced to the 84 m^3 volume AIDA vessel. Subsequently, a scanning mobility particle sizer (SMPS, TSI Inc., Model 3081 Differential Mobility Analyzer, DMA, and Model 3010 condensation particle counter, CPC) and an aerodynamic particle sizer (APS, TSI Inc., Model 3321) were used to measure particle
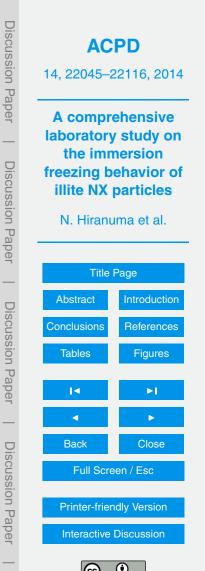
size distributions over the range of 0.01 to 15.4 µm volume equivalent diameter. The assumption of particle sphericity, a dynamic shape factor (DSF or χ in equations) of 1.49 ± 0.12 (average of ten measurements ± standard deviation) and a particle density of $2.65\,\mathrm{g\,cm^{-3}}$ were used to obtain the geometric-based (volume equivalent) diameter from an APS (Hiranuma et al., 2014b). At MRI-DCECC, a combination of a SMPS (TSI Inc., Model 3936) and a welas optical particle counter (welas-OPC, PALAS, Sensor series 2500) was used to acquire a size distribution (0.01 to 47.2 µm volume equivalent diameter) directly from the $1.4\,\mathrm{m^3}$ volume vessel. The same disperser type was used at both chambers for particle generation, and the upstream cyclone impactors ($D_{50} \sim 1\,\mu m$ and 2.5 µm) were similarly deployed to filter out any larger particles and safeguard against injecting these particles into the vessel. We note that a linear correction factor of about two was applied to convert the optical diameter measured by the welas-OPC to the APS-inferred volume equivalent diameter in several studies (Wagner et al., 2011; Hiranuma et al., 2014a).

The particle number size distribution of dry particles in the 0.3-10 µm diameter range was also measured by a TSI 3330 optical particle sizer (OPS, TSI Inc.; TSI-OPS hereafter). For particle generation, the illite NX sample was dispersed using a magnetic stirrer in a 100 mL glass vessel that was purged with $200\,\mathrm{mL\,min^{-1}}$ of dry particle-free compressed laboratory air, and then diluted further in two stages by approximately 1:100 with dry air. Subsequently, the backward scattering intensity of scattered light from a particle illuminated by a laser ($\lambda = 660\,\mathrm{nm}$) is measured. The instrument estimated the particle size distribution, assuming spherical particles, using Mie theory. As a result, the reported size is a volume equivalent spherical diameter.

2.3 Ice nucleation measurements

Table 1 lists the ice nucleation measurement techniques contributing to this collaborative effort. Descriptions of each measurement technique and their acronyms are available in the Supplementary Information. Briefly, four CFDC-type instruments, one continuous flow mixing chamber, two cloud simulation chambers, one diffusion cell,
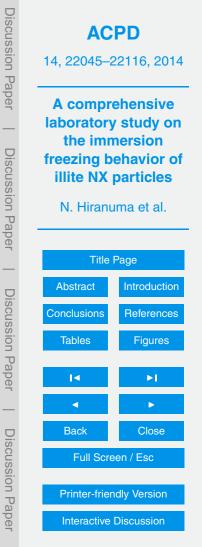
two levitators, one vertical wind tunnel, one laminar flow tube and five cold stage-type systems were employed in the inter-comparison. As seen in the table, measurement techniques with the first seven instruments (i.e., ID 1 to 7) examined droplets produced from bulk illite NX samples in suspension, while the rest used dry-dispersed illite NX powder, sometimes followed by size selection with a DMA. Methods working with suspensions and those using dry particles employ different ways to determine the particle surface area, and the influence of these differences on the determination of n_s was investigated. For instance, CSU-IS was used to investigate the freezing activity of both bulk suspension and size-segregated particles in suspension. Two cloud expansion chambers, AIDA-CECC and MRI-DCECC, examined both polydisperse and size-selected dry illite NX particles. LACIS and IMCA-ZINC measured immersion freezing of droplets, where each one contained a single particle, and examined differently sized dry particles. The role of IN modes upon the estimation of n_s was also examined across various temperature ranges. The EDB-based method was used to measure the contact and immersion mode efficiencies of size segregated dry illite NX particles around −30 °C. Immersion freezing results from IMCA-ZINC were compared to previously reported ZINC data (Welti et al., 2009) at temperatures below −31 °C and to PINC data for temperatures below −26 °C. In the present study, we derived ZINC's n_s values from the results reported in Welti et al. (2009). Specifically, ice formation above 105 % RH_w up to the water drop survival line was used to calculate n_s based on given illite NX particle sizes. We note that the latent heat of condensation has minimal impact on droplet temperature, such that $RH_w > 105$ % maintains a water supersaturating condition for droplet freezing.

FRIDGE investigated ice nucleation of both dry-dispersed particles on a substrate at fixed temperatures (-25 °C $< T < -18$ °C) with increasing humidity ("default" deposition mode nucleation) as well as immersed particles. In the case of immersion freezing experiments with suspended samples, the cell temperature was lowered by 1 °C min^{-1}.

The range of mass concentrations of the bulk illite NX sample in suspension varied from 3.1×10^{-6} wt % (CSU-IS) to 2.6 wt % (M-WT). For dry-dispersed particle mea-

A comprehensive laboratory study on the immersion freezing behavior of illite NX particles

N. Hiranuma et al.

Title Page

Abstract | Introduction

Conclusions | References

Tables | Figures

|◄ | ►|

◄ | ►

Back | Close

Full Screen / Esc

Printer-friendly Version

Interactive Discussion

surements, particle concentrations varied from $\sim 10\,\text{cm}^{-3}$ (AIDA) up to $\sim 9000\,\text{cm}^{-3}$ (MRI-DCECC). Experiments with M-AL, M-WT, EDB, and IMCA-ZINC were performed on a single drop basis. The shortest residence time of roughly one second was used for the laminar flow tube, LACIS, and the slowest cooling rate of $0.3\,^{\circ}\text{C}\,\text{min}^{-1}$ (time-average cooling rate over an expansion, which translates to the equivalent updraft rate of $\sim 0.5\,\text{m}\,\text{s}^{-1}$) was used in AIDA-CECC. Altogether, immersion freezing was examined across the temperature range from ~ -10 to $\sim -38\,^{\circ}\text{C}$, and over a varied range of cooling rates, nucleation times and particle concentrations (summarized in publically accessible data base available at http://imk-aaf-s1.imk-aaf.kit.edu/inuit/).
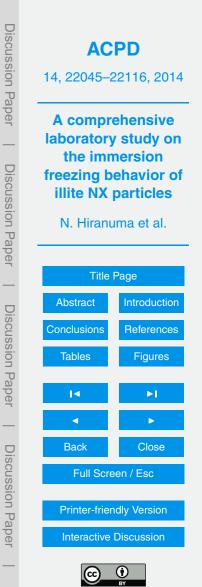
2.4 Ice nucleation parameterization

We now describe a method to parameterize surface area-scaled immersion freezing activities using the size equivalent ice nucleation active surface-site density (Connolly et al., 2009; Niemand et al., 2012; Hoose and Möhler, 2012), relating it to the geometrically determined surface area, $n_{\text{s,geo}}$. In short, this surface-site density approach approximates ice crystal formation (in n bins of particle size distribution measurements) observed in an experiment as a function of temperature, thus not accounting for time-dependence. Accordingly, $n_{\text{s,geo}}$ can be expressed by:

$$
n_{\text{s,geo}}(T) = J_{\text{imm}}t = -\ln\left(1 - \frac{\sum\limits_{i=1}^{n} N_{\text{ice},i}}{\sum\limits_{i=1}^{n} N_{\text{total},i}}\right)\left(\frac{1}{S_{\text{ve},i}}\right), \tag{1}
$$

in which, J_{imm} is the immersion freezing rate coefficient ($\text{m}^{-2}\,\text{s}^{-1}$), $N_{\text{ice},i}$ is the number concentration of formed ice crystals in size bin i (cm^{-3}), $N_{\text{total},i}$ is the total number concentration of particles prior to any freezing event in size bin i (cm^{-3}), and $S_{\text{ve},i}$ is the volume equivalent surface area of individual particles in size bin i (m^2). As demon-

strated in Niemand et al. (2012), if the activated ice fraction is small (< 0.1), the Taylor series approximation can be applied to Eq. (1). Assuming a uniform distribution of $n_{s,geo}$ over a given S_{total} and a size-independency of $n_{s,geo}$, we can approximate $n_{s,geo}$ as:

$$n_{s,geo}(T) \approx \frac{\sum\limits_{i=1}^{n} N_{ice,i}}{\sum\limits_{i=1}^{n} N_{total,i}S_{ve,i}} = \frac{N_{ice}(T)}{S_{total}}. \tag{2}$$

In addition, the IN efficiency can be related to the BET-SSA to estimate BET-inferred ice nucleation surface-site density, $n_{s,BET}$, under water suspended conditions. A description of the procedures used to estimate both n_s metrics is given in Hiranuma et al. (2014b). The advantage of using $n_{s,geo}$ is its applicability to both measurements and modeling activities due to the assumption of particle sphericity. Conversely, $n_{s,geo}$ cannot be directly obtained through suspension experiments because the size distribution of a suspended sample for each experiment is not available, therefore S_{total} is determined from BET and the sample mass suspended in water.
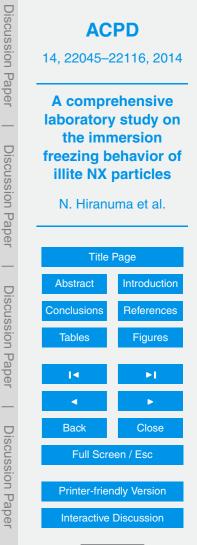
In order to convert $n_{s,geo}$ values of all dry-dispersed particle measurements into $n_{s,BET}$, the following procedure is used: First, geometric size-based ice nucleating mass, $n_{m,geo}$ (g^{-1}), was calculated from IN active surface using either the surface-to-mass conversion factor (in $m^2\,g^{-1}$) of $6/D_{ve,i}\rho$ (size-selected case) or S_{total}-to-M_{total} (polydisperse case) by:

$$n_{m,geo}(T) = \frac{\sum\limits_{i=1}^{n} N_{ice,i}}{\sum\limits_{i=1}^{n} N_{total,i}M_{ve,i}} = \frac{6}{D_{ve,i}\rho}n_{s,geo}(T) \approx \left(\frac{S_{total}}{M_{total}}\right)n_{s,geo}(T) \tag{3}$$

where $M_{ve,i}$ is the mass of a spherical particle of volume-equivalent diameter in size bin i (g), $D_{ve,i}$ is the volume equivalent midpoint diameter of particles in size bin i (m), ρ is
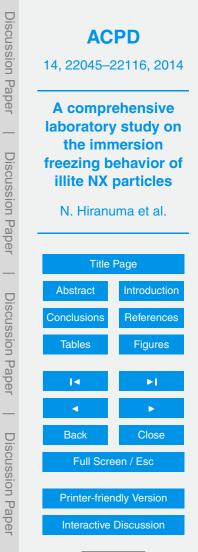
the particle density of illite NX (2.65×10^{6} g m^{-3}), and M_{total} is the total particle mass (g cm^{-3}). We note that the DLS size distribution derived S_{total}-to-M_{total} ratio (i.e., DLS-SSA) was 6.54 m^{2} g^{-1} and used for the measurements with polydispersed particles. We also note that the conversion factor ranged from 11.3 to 2.26 m^{2} g^{-1} for size-selected

5 particle diameters from 200 nm to 1000 nm, respectively, where these sizes denote the range of particle diameters used in the size-selected cases in the present study. Lastly, ice nucleating mass was scaled to the BET-SSA (θ, 124.4 m^{2} g^{-1}) to derive $n_{s,BET}$ as:

$$n_{s,BET}(T) = \frac{n_{m,geo}(T)}{\theta} \approx \frac{n_{m,sus}(T)}{\theta} = \frac{\alpha}{M_{ve,i}\theta} \qquad (4)$$

10 in which, $n_{m,sus}$ is the IN active mass for suspension measurements, α represents the ice activated fraction (= N_{ice} / N_{total}), which is the direct measurement of suspension experiments and some of the dry-dispersed particle methods. Owing to internal surface area and surface roughness, BET-SSA may be greater than DLS-SSA (O'Sullivan et al., 2014). Agglomeration can further reduce the effective surface area exposed to air

15 or available to water. The usage of DLS-SSA appears to be reasonable, as this leads to an $n_{s,geo}$ for suspension measurements nearly equivalent to $n_{s,geo}$ for dry-dispersed particles. When the S_{total}-to-M_{total} ratio is derived based on TSI-OPS measurements, a value of 0.49 m^{2} g^{-1} is obtained, which is larger by a factor of about thirteen compared to the above given value, where the latter was used for the data evaluation through-

20 out this study. The resulting $n_{s,BET}$ is especially representative of measurements with suspended samples because minimal corrections (only α and θ) are involved when compared to that with dry-dispersed particles. Hence, the use of $n_{s,BET}$ is appropriate for our instrument comparison study. Alternatively, we can also convert ice nucleating mass derived from suspension measurements, $n_{m,sus}$, to $n_{s,geo}$ using hydrodynamic

25 size distributions of illite NX particles in water suspension with the DLS technique, to provide a reasonable comparison to dry-dispersed particle measurements. However, it is one step further when compared to $n_{s,BET}$ (with an additional assumption of constant size distribution for all suspensions) and two steps further compared to n_{m}. For
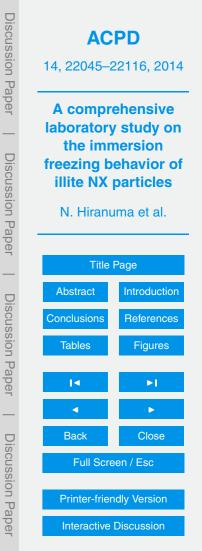
our inter-comparison study, we used both $n_{s,BET}$ and $n_{s,geo}$. Because fewer conversion factors are involved, $n_{s,BET}$ is more representative for suspensions and $n_{s,geo}$ is better for dry-dispersed particle measurements (Eqs. (3) to (4) or vice versa).

3 Results

3.1 Illite NX characterization

XRD results from the present and previous studies (Friedrich et al., 2008; Broadley et al., 2012) of the major minerals in bulk samples of illite NX are presented in Table 2. The results show that the bulk illite NX powder is composed of various minerals: illite, kaolinite, quartz, calcite and feldspar, but the relative mass of these minerals differed from previous studies. For example, our measurement shows that the illite NX sample was composed of ∼ 69 wt % illite mineral, whereas others reported a larger amount of illite from 74 to 86 wt %. Similarly, we observed a somewhat different content of other minerals compared to previous studies as listed in Table 2 (see also Fig. S1 in the Supplement). We note that the fractional values in compositional fingerprints may deviate even within the same batch, as all three XRD measurements deviated from the manufacturer's data (Table 2). Furthermore, our XRD result indicates that the illite NX sample contains a smaller quartz fraction (3 %) than IMt1-illite from the Clay Mineral Society (10 to 15 % quartz according to the official XRF data and 20 % based on our own measurements).
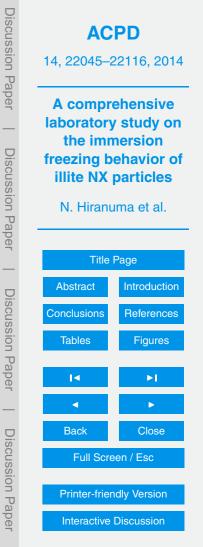
To complement bulk XRD analysis, the wt % of thirteen elements (Pt, K, C, Ca, O, Fe, Mg, Al, Si, P, S, Pb and Ti), which are commonly identified in illite-rich samples, was measured by EDX spectroscopy on a single particle basis. Four representative EDX spectra are presented in Fig. 1. The presence of Fe and Mg is typical and characteristic for illite NX particles. The observed large amounts of Si and Al are due to the presence of layered aluminosilicate structures (i.e., layer of SiO_2 and Al_2O_3). The observed dominant platinum (Pt) signals in all spectra originate from the sputter coating

conducted prior to EDX analyses. Figure 1A shows the typical illite spectrum, which is similar to the one published elsewhere (Welton, 1984). Illite-rich minerals, which included impurities of calcite, TiO_2 and Pb-P, were located by the brightness difference in the backscattered electron detector micrograph images, and are shown in Fig. 1b,

5   c and d, respectively. However, the EDX technique is not automated to detect these impurities present within the illite NX particles because of their very small weight fraction. Therefore, the possible effect of impurities upon the ice nucleation activity cannot be evaluated on the basis of a bulk analysis of the chemical composition. Nonetheless, detection of non-illite mineral components implies the possibility of a wide range

10 of ice nucleation efficiencies by the test sample at various temperatures. Hence, the illite NX sample may reflect the complexities of natural dust particles, which typically contain multiple sites with differing nucleation abilities, and can therefore be used as a reference material to mimic ice nucleation activity of physically and chemically complex natural dusts.

15   The measured BET-SSA are 124.4 and 123.7 $m^2 g^{-1}$ with N_2 and H_2O vapor respectively as the adsorbing gas on illite NX particle surfaces. The similar BET surface areas for both N_2 and H_2O vapor gas adsorption suggests that the formation of a few monolayers of H_2O does not alter the surface morphology or the mineralogical phase of illite NX particles. For comparison, our measurements of θ_{N_2} for illite NX particles agreed

20 with previously reported data within ± 20 % (104.2 $m^2 g^{-1}$; Broadley et al., 2012). Illite NX particles have significant internal surface area and BET surface areas can be expected to yield a much greater surface area than the laser diffraction technique. To support this, a SEM image of an illite NX particle from Broadley et al. (2012) shows how micron scaled particles are made up of many nanometer sized grains.

25   Normalized surface area distributions measured by four different techniques are shown in Fig. 2. According to the manufacturer, 95 % mass of dry and mechanically de-agglomerated illite NX particles have a diameter smaller than 650 nm (i.e., D_{95}). These mass-based particle size is substantially smaller than that of another type of Arginotec illite (Arginotec, SE-illite, $D_{95} = 5 \mu m$). Interestingly, all mass size distribu-
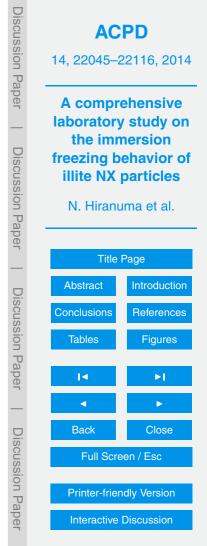
tions (not shown here) indicate substantial mass fraction above 650 nm which is, in all cases, larger than 5 % (18, 24, 77 and 99.9 % for DLS, AIDA, MRI-DCECC and TSI-OPS, respectively), indicating the presence of agglomerates in the aerosol and suspension phases prepared for the IN experiments. The surface area distribution of the DLS hydrodynamic diameter-based measurement (Fig. 2a) agreed well with in situ measurements from the AIDA chamber (Fig. 2b), suggesting the size distributions of dry illite NX particles during AIDA experiments were similar to those of suspension measurements. The wider distributions and the shift in the mode diameter in MRI-DCECC towards larger size (0.62 µm, Fig. 2c) when compared to Fig. 2a and b may indicate a higher degree of particle agglomeration as a result of incomplete pulverization during the particle generation processes or particle coagulation at the high aerosol number concentration. In Sect. 4.4 we discusses whether agglomeration has an effect on the IN activity. A more pronounced agglomeration effect was observed by the TSI-OPS measurements (Fig. 2d), such that increased area concentrations of supermicron particles were obtained.

The cation release by illite NX in the aqueous suspension was measured with IC as a function of time. The suspension was kept mechanically agitated for 3 weeks. The following cations have been identified in the samples: K^+, Na^+, Ca^{2+}, and Mg^{2+}. As seen in Fig. 3, IC data clearly demonstrate that all cations were released into the aqueous environment by illite NX almost instantaneously. The concentration of the cations increases rapidly and reaches equilibrium within the first 2 min after immersion of sample into water. Of all the cations measured, only Ca^{2+} exhibits a slow concentration raise on the longer time scales.

3.2 Immersion freezing measurements and inter-comparisons

Figures 4 and 5 show all ice nucleation spectra with $n_{s,BET}(T)$ and $n_{s,geo}(T)$, respectively. A similar figure with $n_m(T)$ is also shown in the Supplemental Figure S2. Furthermore, we compare the n_s data from seventeen instruments to four literature results. Specifically, reference curves of previously reported illite NX particles (Broadley et al.

2012, hereafter B12), microcline particles (Atkinson et al., 2013, hereafter A13), ATD and desert dusts (Niemand et al., 2012, hereafter N12) are also expressed as both $n_{s,BET}(T)$ and $n_{s,geo}(T)$. The conversion between $n_{s,geo}(T)$ and $n_{s,BET}(T)$ was performed according to Eqs. (3) and (4). The $n_s - T$ (m^{-2} °C) fits from the previous literatures are:

$$n_{s,BET}^{A13} = 10^4 \times \exp\left(-1.038\,(T - 273.150) + 275.260\right) \tag{5}$$

$$n_{s,BET}^{B12} = 10^4 \times \exp\left[\left(6.530 \times 10^4\right) + \left(\left(-8.215 \times 10^2\right) \times (T - 273.150)\right)\right. \tag{6}$$
$$\left. + \left(3.447 \times (T - 273.150)^2\right) + \left(\left(-4.822 \times 10^{-3}\right) \times (T - 273.150)^3\right)\right]$$

$$n_{s,geo}^{N12(ATD)} = \exp\left(-0.380T + 13.918\right) \tag{7}$$

$$n_{s,geo}^{N12(Dust)} = \exp\left(-0.517T + 8.934\right). \tag{8}$$

For K-feldspar, the $n_{s,geo}$ to $n_{s,BET}$ conversion was performed using a laser diffraction-based surface-to-mass conversion factor of 0.89 m^2 g^{-1} and a N$_2$ BET-SSA of 3.2 m^2 g^{-1} (Atkinson et al., 2013). For ATD and natural dust, we used a surface-to-mass conversion factor of 3.6 m^2 g^{-1}, assuming a monodisperse particle size at the lognormal fit mode diameter of 0.64 µm (Niemand et al., 2012) and the measured N$_2$ BET-SSA of 34.4 m^2 g^{-1} (this study). We note that the ATD parameterization is valid only for $-26.7\,°C < T < -17.7\,°C$. In addition, we also present 14 %, 0.14 % and 0.0014 % scaled A13 n_s curves to see if K-feldspar (microcline) can be used as a scaling factor to determine the $n_s(T)$ of illite NX (i.e., up to 14 %).

We do not attempt to completely discuss the immersion freezing activity of illite NX particles measured by each measurement technique. Instead, brief remarks from each experiment are summarized below. The detailed discussion of the methods intercomparison follows in Sect. 3.3.

3.2.1 BINARY

This recently developed microliter droplet assay technique demonstrated its capability of measuring immersion freezing of clay minerals in the temperature range between −15 and −24 °C. Similar to most of the other suspension based techniques, BINARY identified the steep n_s increase, which starts just below −20 °C. The BINARY $n_s(T)$ spectrum was derived by compiling measurements with varied illite NX mass concentration over two orders of magnitude (0.1 to 10 mg mL^{-1}, see the Supplement methods). Immersion freezing efficiency of illite NX particles collapsed into a single $n_s(T)$ spectrum, suggesting that IN efficiency does not depend on suspended particle mass for the concentration range studied here.
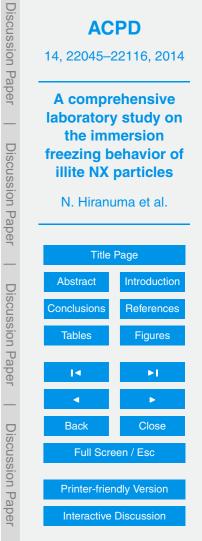
3.2.2 CSU-IS

This new immersion freezing device was used to investigate the freezing activity of both bulk suspension and size-segregated particles in suspension. A new approach was employed for size-selected measurements, wherein 500 nm mobility diameter size particles were collected on a Nuclepore filter and then rinsed from it for the immersion freezing measurements. The results suggested size-independence of n_s within the experimental uncertainties (a combination of binomial sampling error and the uncertainty of conversion of aerodynamic particle diameter to mass) for the range of examined mass concentrations of bulk illite NX powder in suspensions (from 3.1×10^{-6} to 0.5 wt %, for non-size-segregated particles, and 2.2×10^{-5} to 4.4×10^{-4} wt % for size-segregated particles).

3.2.3 Leeds-NIPI

This suite of cold stage instruments has the capacity to operate with droplets of volume from micro-liter to pico-liter. This enables high resolution immersion freezing analysis for a wide range of temperatures from higher (−22 °C < T < −11 °C) to lower temper-

Title Page

Abstract | Introduction

Conclusions | References

Tables | Figures

|◄ | ►|

◄ | ►

Back | Close

Full Screen / Esc

Printer-friendly Version

Interactive Discussion

atures ($-37\,°C < T < -26\,°C$); with the highest temperatures attained with the largest droplets which contain the largest surface area of illite NX. Combined with the previous parameterization reported in Broadley et al. (2012), the Leeds-NIPI data follows the overall $n_s(T)$ spectrum defined by the bulk of the instruments. This suggests that immersion freezing efficiency, inferred by ns(T), of illite NX particles is dependent on neither droplet volume nor mass of illite NX particles in suspension (i.e., wt % 0.1 or 1 %); instead the freezing efficiency only depends on the surface area per droplet. Together with CSU-IS, these two instruments provided data points for temperature as high as $\sim -11\,°C$, estimating similar lower-limit $n_{s,BET}$ values of $\sim 10\,m^{-2}$.
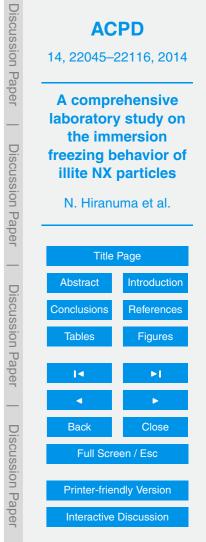
3.2.4 M-AL and M-WT

Both methods examined individual drops that are freely suspended without any contact with walls or substrates. In M-WT drops are floated at their terminal velocities in a laminar air stream, in which conditions of ventilation and heat transfer are similar to those of droplets falling through the atmosphere. Both M-AL and M-WT techniques analyzed the freezing efficiency of drops containing polydisperse illite NX particles in the temperature range between -14 and $-26\,°C$. The n_s values agree reasonably well with substrate-supported suspension experiments (with an exception of FRIDGE), implying that the absence of an effective surface in contact with a substrate has a negligible effect on immersion freezing for our experimental conditions.

3.2.5 NC State-CS

Extensive experimental conditions were realized by NC State-CS (Wright and Petters, 2013; Hader et al., 2014). Unique aspects of this instrument are the sampling of drops within a squalene oil matrix to allow for experiments using cooling rates as slow as $0.01\,K\,min^{-1}$ and an automated freeze detection algorithm that allows processing of more than 1000 drops per experiment to improve sample statistics. Drops containing ~ 0.0001 to $1.0\,wt\%$ of the illite NX test sample were studied at a cool-

ing rate of $1\,\mathrm{K\,min^{-1}}$ to find the immersion freezing ability. A total of nine immersion mode freezing experiments, spanning a range of drop volumes from $\sim 400\,\mathrm{pL}$ to 150 nL, were performed. Using this instrument a wide range of temperatures was investigated ($-34\,^{\circ}\mathrm{C} < T < -14\,^{\circ}\mathrm{C}$) yielding $n_\mathrm{s}(T)$ values ranging from 10^2 to $10^{10}\,\mathrm{m^{-2}}$. The data from the nine individual runs collapsed into a single horizontally flipped S-shape $n_\mathrm{s}(T)$ spectrum suggesting that the mass loading of dust in the drop does not affect the measurements for the wt % values investigated. At the warm end, $T > -20\,^{\circ}\mathrm{C}$, the data are in reasonable quantitative agreement with the CSU-IS measurements. At the cold end ($T < -20\,^{\circ}\mathrm{C}$) the data are in agreement with the B12 reference spectrum.
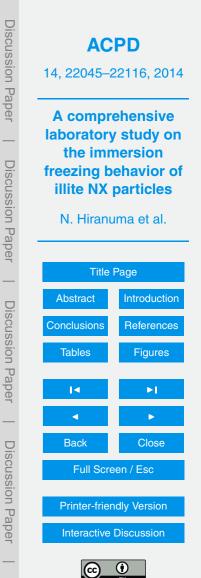
3.2.6 CU-RMCS

The University of Colorado (CU)-RMCS examined the freezing potential of droplets containing 1.0 wt % NX-illite. Results for $-32 < T < -23\,^{\circ}\mathrm{C}$ are from 6 different experiments using 4 different droplet size bins: 10–20 µm, 20–60 µm, 60–120 µm, and 120–200 µm (lateral diameter). These droplet sizes correspond to a variation in droplet volume from ~ 0.3 picoliter to 2.5 nanoliter.

3.2.7 AIDA

The AIDA cloud simulation chamber generates atmospherically relevant droplet sizes (several µm in diameter, varying with cooling rates), and therefore closely simulates mixed-phase cloud conditions. n_s of size-selected illite NX particles (200, 300 and 500 nm mobility diameter) agreed well with that of the polydisperse population within previously reported uncertainties for immersion freezing experiments ($T \pm 0.3\,^{\circ}\mathrm{C}$ and $n_\mathrm{s} \pm 35\,\%$; Steinke et al., 2011). Thus, a negligible size-dependency of n_s for submicron dry illite of NX particles for temperatures below $-27\,^{\circ}\mathrm{C}$ was found.
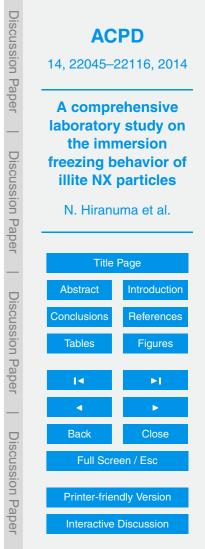
3.2.8 CSU-CFDC

This CFDC provided data for condensation/immersion freezing in the temperature range of $-29.7\,°C < T < -21.2\,°C$, which extends to a warmer region than AIDA measurements. As demonstrated in DeMott et al. (2014), the higher RH_w values required for full expression of immersion freezing in the CFDC. The use of 105 % RH_w in CSU-CFDC does not capture up to a factor of three INP activity for many natural dusts. Comparably, CSU-CFDC agreed well with AIDA measurements within a factor of three in $n_{s,geo}$ estimation (AIDA n_s > CSU-CFDC n_s; DeMott et al., 2014).

3.2.9 EDB

With EDB, both the contact and immersion mode freezing efficiencies of illite NX particles were investigated. The contact nucleation mode n_s were clearly higher than the immersion mode n_s (by more than one order of magnitude in terms of $n_{s,geo}$, Fig. 5i). This is in part due to the fact that immersion freezing experiments were conducted only when illite NX particles were not frozen via the contact nucleation but remained available immersed in a supercooled droplet in the EDB cell (see the Supplement method). A more detailed discussion of comparison between contact mode and immersion mode freezing efficiencies of illite NX particles is available in Sect. 4.5.

3.2.10 FINCH

The immersion freezing results from FINCH showed the highest n_s values in the -27 to $-22\,°C$ temperature range. All the FINCH measurements were conducted with 500 nm mobility diameter size-selected particles. Two possible reasons for the discrepancy are: (1) an overestimation of n_s due to excess N_{ice} or underestimated S_{total} or (2) a temperature-uncertainty. It is noteworthy that the total INP concentration was kept below 140 L^{-1} in order to avoid saturation limitation due to a high number of growing ice crystals (DeMott et al., 2011). A constant total concentration of particles continuously

passing through the chamber was maintained at $1.07 \pm 0.17\,\mathrm{cm}^{-3}$ (average ± standard deviation).
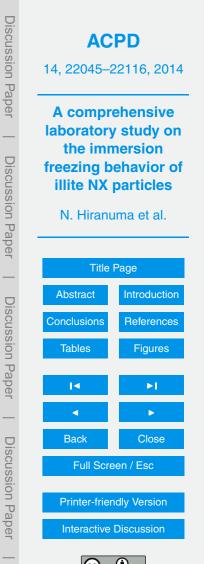
3.2.11 FRIDGE

FRIDGE data, which cover both measurements of dry and immersed particles with the same instrument but with different sample processing, lie within the upper edge of the bulk of other n_s data points. There are a few important implications from the FRIDGE results. First, on average, the measurements with dry particles showed an one order of magnitude higher n_s (both $n_{s,\mathrm{BET}}$ and $n_{s,\mathrm{geo}}$, Figs. 4 and 5) at $-25\,^{\circ}\mathrm{C} < T < -18\,^{\circ}\mathrm{C}$. For instance, FRIDGE experiments in the pure immersion mode showed much lower n_s than that with the "default" setting (i.e., combined deposition and immersion mode), but agreed with other immersion datasets. Second, a sudden decrease in $n_s(T)$ was found for the measurements with immersed particles at $-20\,^{\circ}\mathrm{C}$, suggesting a dominant activation around $-20\,^{\circ}\mathrm{C}$. This transition is a unique behavior only found with the FRIDGE's IN detecting sensitivity. A temperature shift (i.e., shifting the data $\sim 7\,^{\circ}\mathrm{C}$ lower) results in FRIDGE data overlapping with the bulk of other data and may offset discrepancies. However, other mechanistic interpretations (e.g., contribution of agglomeration) are also plausible causes of this discrepancy. The more detailed discussions of the role of agglomerates upon n_s and sample-processing (i.e., dry vs. suspension sample) are available in Sects. 4.4 and 4.5.

3.2.12 LACIS

With the shortest instrument residence time ($\sim 1.6\,\mathrm{s}$), LACIS measured immersion mode freezing of illite NX particles for three different mobility diameters (300, 500 and 700 nm) below $-31\,^{\circ}\mathrm{C}$ down to the homogeneous freezing temperature. Similar to AIDA results, a size-independence of n_s of submicron illite NX particles was observed within defined experimental uncertainties (see the Supplement Method). Further, without any data corrections, the results of LACIS reasonably agreed with AIDA measurements.
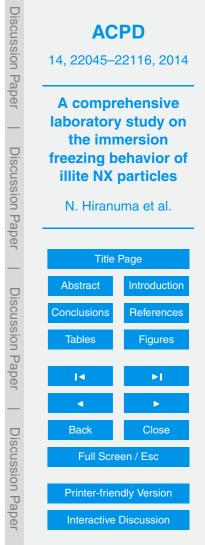
Furthermore, though there is no overlapping temperature range for LACIS and CSU-CFDC in the present study, consistency between data from LACIS and CSU-CFDC for other clay minerals (i.e., different kaolinite samples) has been described previously (Wex et al., 2014). The results from both instruments agreed well with each other for a data evaluation based on n_s and, with a slightly better agreement, a time-dependent treatment.

3.2.13 MRI-DCECC

Comparison between polydisperse and size-selected (300 nm mobility diameter) measurements in this cloud simulation chamber demonstrated the size-independency of n_s for submicron illite NX particles for slightly higher temperatures (up to $-21\,°C$) than AIDA results. Interestingly, MRI-DCECC data exhibited at least an order of magnitude higher n_s values from most other suspension measurements. We note that only negligible freezing events were detected above $-21\,°C$ even with a $\sim 9000\,cm^{-3}$ number concentration of polydisperse illite NX particles (i.e., MRI-DCECC) due to the detection limit of the welas optical counter, which is N_{ice} of $0.1\,cm^{-3}$.

3.2.14 PINC

The estimated n_s values are in agreement with other measurements for their test range of $-35\,°C < T < -25\,°C$ after applying a residence time correction of about a factor of three. The data are for ice nucleation onto 500 nm and 1000 nm (mobility diameter) illite NX particles, therefore an OPC threshold size of $2\,\mu m$ for ice detection is used. The impactor used for sampling particles into PINC was characterized for size-resolved particle losses and was found to have a cutoff (D_{50}) of 725 nm (mobility diameter). As such when determining $n_{s,geo}$ the particles losses (25 to 60 %, see Supplement Method for more details) were taken into account for calculating activated fractions. We note that $n_{s,geo}$ increased after adjusting the data, resulting in the data from PINC being

in agreement with LACIS, AIDA and UC-RMCS in the temperature range from -25 to $-35\,°C$.

3.2.15 PNNL-CIC

The efficiency of illite NX particles to nucleate ice via immersion freezing was observed to increase at lower temperatures. Estimated n_s values were somewhat higher when compared to other measurements. Data were obtained at conditions where PNNL-CIC was operated 105 % RH$_w$ at three different temperatures. Dust particles greater than $\sim 1\,\mu m$ (50 % cut size) were removed before they were size-selected and transported to the PNNL-CIC. The OPC detection threshold was set $\geq 3\,\mu m$, see Supplementary Method section for more details.

3.2.16 IMCA-ZINC

Coupled with IMCA, ZINC showed reasonable agreement with AIDA and PNNL-CIC. This reproducibility verified the performance of the IMCA-ZINC combination, which was not tested during ICIS-2007 (DeMott et al., 2011), perhaps due to the similarity in the experimental conditions (i.e., particle generation) to the other two methods. We also note that the residence time in ZINC is about a factor of 3 longer than that in PINC. Comparison to the measurements with ZINC alone (i.e., a combination of deposition nucleation, contact/condensation/immersion freezing and surface condensation freezing; Welti et al., 2009) is discussed in Sect. 4.5 in more detail.

As described above, suspension experiments with cold stage devices and levitation techniques provided IN measurements under more controlled (i.e., droplet size, concentration and mass of particles) conditions and a wider temperature range (up to $-11\,°C$) warmer than comparable dry-dispersed particle experiments. The resulting n_s values from these suspension experiments are also independent of the total number of droplets and suspended dust particle mass.
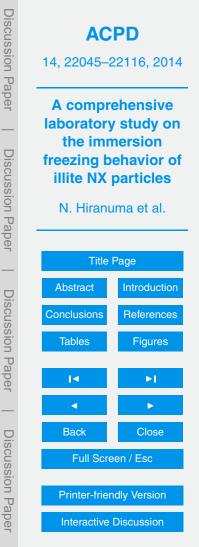
The estimated n_s values of dry test particles were in reasonable agreement with a previous study (Broadley et al., 2012) at temperatures below −25 °C. Furthermore, the strong temperature-dependence and size-independence of n_s suggested a uniform distribution of freezing sites over the total surface of illite NX particles in the immersion mode in this temperature range. Specifically, a number of instruments (AIDA, LACIS, MRI-DCECC, PINC, PNNL-CIC and IMCA-ZINC) have shown size-independent n_s values for dry-dispersed particles. Overall, compared to suspension measurements, dry-dispersed particle measurements showed more pronounced diversity between measurements. For example, FINCH is the only instrument which showed higher n_s values than the parameterization by Niemand et al. (2012) for ATD. Likewise, AIDA results indicated slightly higher n_s than CSU-CFDC's data points. The lower n_s of CSU-CFDC may be a consequence of underestimation of N_{ice}, possibly due to its constrained RH_w (at 105 %) and/or the disturbance of aerosol lamina between two plates in a CFDC (DeMott et al., 2014). In-depth discussions of potential reasons for diversity specific to dry-dispersed particle measurements are given below (Sect. 4.).

3.3 Comparison to literature results with the slope parameter of n_s(T) spectra

Figure 6 shows a compilation of seventeen n_s spectra from seventeen instruments in a temperature range between −10.1 and −37.5 °C. For both the geometric area-based and the BET area-based n_s, the differences among measurements can be more than one order of magnitude at any given temperature. Diversity is especially pronounced (for several orders of magnitude in n_s) at $-27\,°C < T < -18\,°C$, where the results from suspension measurements and dry measurements coexist. Another notable feature of this specific temperature range in Fig. 6 is the coincidence of the steepest slope in the spectrum (i.e., $\Delta\log(n_s)\,/\,\Delta T$ in $\log\text{m}^{-2}\,°C^{-1}$) when compared to other temperature ranges. For instance, n_s increases sharply to be nearly parallel to the A13 parameterization down to −27 °C, starts leveling off afterwards and is eventually overlapping with the N12 parameterization at the low temperature segment.

Title Page

Abstract | Introduction

Conclusions | References

Tables | Figures

|◄ | ►|

◄ | ►

Back | Close

Full Screen / Esc
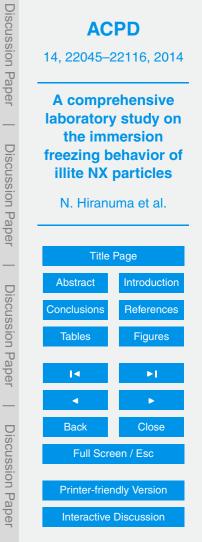
Printer-friendly Version

Interactive Discussion

Correspondingly, the overall trend of a spectrum was traced by the measurements from NC State-CS alone (Fig. 4e). Moreover, the slopes of the spectrum for three sub-segments ($-34\,°C < T < -27\,°C$, $-27\,°C < T < -20\,°C$, and $-20\,°C < T < -14\,°C$) were calculated from interpolated data and compared to N12 and A13 parameterizations. As expected, the steepest slope (= 0.66) of NC State-CS data was found for $-27\,°C < T < -20\,°C$, which was similar to A13 (0.45 for $-25\,°C < T$), whereas rather smaller values were found for the other two segments (0.18 for $T < -27\,°C$ and 0.29 for $-20\,°C < T$) which were comparable to the temperature-independent N12 slopes (0.17 for ATD and 0.22 for Dust) and the B12 slope (0.25 for $-35\,°C < T < -27\,°C$), suggesting that a large fraction of active sites of our test dust may trigger immersion freezing at $-27\,°C < T < -20\,°C$. In addition, FRIDGE immersion mode measurements also identified a sharp decrease in $\Delta\log(n_s)\,/\,\Delta T$ (from 0.59 to 0.25, Figs. 4k and 5k) for the measurements with immersed particles at $-20\,°C$. Similar observations were made by most of the other suspension measurement techniques except CU-RMCS, which detected first immersion freezing of illite NX particles at about $-23\,°C$ under its experimental conditions used in the present work (see Supplementary Method).

In short, most suspension methods captured the steepest segment of the $n_s(T)$ spectral slopes ($\Delta\log(n_s)\,/\,\Delta T$) at $-27\,°C < T < -20\,°C$, where the slope is nearly parallel to the A13 parameterization. One exception is CU-RMCS (Fig. 4f). The highest possible freezing temperature investigated by this experimental system was about $-23\,°C$ with ~ 2.5 nanoliter droplets containing 1.0 wt % illite NX. Hence, CU-RMCS did not capture the transition in $\Delta\log(n_{s,BET})/\Delta T$ at around $-20\,°C$, but the steep slope of the spectrum (= 0.36) validated the high density of IN active sites below $-23\,°C$. The error in temperature for this technique is always $\pm 0.5\,°C$, based on the freezing experiments without any foreign substances in supercooled drops (i.e., homogeneous freezing experiments).

Dry-dispersed particle measurements exhibited more scattered data for their measured temperature ranges when compared to suspension measurements. Both agreements and equally important disagreements were observed. First, the agreements are
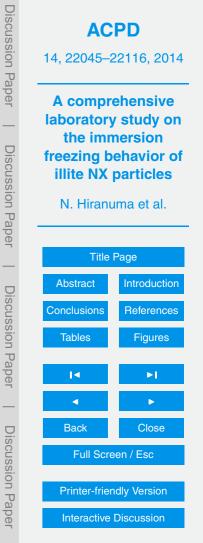
summarized. AIDA data showed that the values of $\Delta \log(n_{s,geo}) / \Delta T$ (= 0.22, Fig. 5g) were identical for both polydisperse and size-selected measurements, suggesting a uniform distribution of active sites over the available S_{total}. Similarly, IMCA-ZINC's $\Delta \log(n_{s,geo}) / \Delta T$ (= 0.24, Fig. 5p) derived from 200 nm, 400 nm and 800 nm mobility di-
ameters is identical to the slope estimated from AIDA measurements. PINC estimated $\Delta \log(n_{s,geo})/\Delta T$ (= 0.26, Fig. 5n) values are in reasonable agreement with AIDA and IMCA-ZINC and N12 parameterizations at temperatures below $-25\,^{\circ}$C. From the CSU-CFDC results, $\Delta \log(n_{s,geo})/\Delta T$ derived from interpolated data was 0.40 (Fig. 5h). To-gether with AIDA data, the $n_s(T)$ spectrum depicts similar trends (i.e., n_s or temperature
deviation around $-27\,^{\circ}$C) compared to those seen in the NC State-CS results (Fig. 5e) and is also parallel to the A13 curve (slope = 0.45) down to temperatures around $-27\,^{\circ}$C followed by the N12 Dust curve (slope = 0.22) for the lower temperature seg-ment. LACIS measurements showed that $\Delta \log(n_{s,geo}) / \Delta T$ (= 0.19, Fig. 5l) is also in agreement with that from AIDA, verifying a deteriorated freezing ability of illite NX par-
ticles in the investigated temperature range. EDB was used to examine both contact and immersion modes. Nonetheless, the slopes of the spectra for both modes (0.11 for immersion mode freezing and 0.16 for contact mode freezing, Fig. 5i) were similar to the N12 ATD curve (slope = 0.17). From the fact that the value of $\Delta \log(n_{s,geo}) / \Delta T$ of FINCH (= 0.27, Fig. 5j) above $-27\,^{\circ}$C is similar to that of the N12 parameterization,
which should coincide with T below $-27\,^{\circ}$C, we suspect that a temperature uncertainty may be the main cause of the observed deviation of its data from others. Lastly, at $-35\,^{\circ}$C $< T < -27\,^{\circ}$C, PNNL-CIC's $\Delta \log(n_{s,geo}) / \Delta T$ (= 0.19, Fig. 5o) well agreed with that from the N12 parameterization in the same temperature range.

Next, the unique results of dry-dispersed particle measurements are presented.
Specifically, MRI-DCECC identified lower values of $\Delta \log(n_{s,geo})/\Delta T$ (= 0.29) up to $-21\,^{\circ}$C as compared to the suspension measurements. This observation is very inter-esting because a more pronounced immersion activation above $-21\,^{\circ}$C (i.e., higher $n_s(T)$ at $T < -21\,^{\circ}$C) opposes the observation made from suspension data and the associated sharp transition in $\Delta \log(n_s)/\Delta T$. We note that MRI-DCECC experiments

Title Page

Abstract	Introduction
Conclusions	References
Tables	Figures

|◄ ►|

◄ ►

Back Close

Full Screen / Esc

Printer-friendly Version

Interactive Discussion

were carried out with the presence of a high degree of agglomerates (Fig. 2c and d). Hence, particle processing (i.e., dry and suspended) may not be the only factor causing this difference and other contributions cannot be ruled out. For instance, the higher n_s when compared to others may be indicative of a higher degree of agglomeration (see
5 Sect. 4.4).

To conclude, the results from suspension and dry measurements suggest evidence that immersion freezing n_s of illite NX particles is independent or only weakly dependent on droplet size, mass percent of illite NX sample in suspension and droplets, particle size of the tested illite NX and cooling rate during freezing relative to the range of
10 conditions probed (see the Supplement Methods for more detailed information regarding experimental conditions for each instrument). Our results constrain the n_s concept by premising a uniform distribution of active sites for available S_{total}, strong temperature-dependency and relatively weak time-dependency of immersion freezing for illite rich clay mineral particles. Overall, the sample-processing (i.e., dry vs. suspension sample)
15 may have an effect on the immersion freezing efficiency of illite clays. A more detailed discussion will follow in Sect. 4 below.

4 Discussion

For detailed comparison of methodologies, the immersion freezing properties of illite NX particles, in a wide range of temperatures, was elucidated by comparing $n_s(T)$
20 spectra of all seventeen instruments (Sect. 4.1). Specifically, we present T-binned average data (i.e., 1 °C bins for -37 °C $< T < -11$ °C). Moving average (where original data points are finer than 1 °C) or Piecewise Cubic Hermite Interpolating Polynomial function (where original data points are coarser than 1 °C) were used for data interpolation. All data from the seventeen instruments, as shown in Fig. 4, were interpolated.
25 We also discuss potential reasons for diversity observed from inter-comparisons of dry and suspension measurement techniques. Both systematic errors (Sect. 4.2) and mechanistic uncertainties (Sect. 4.3 to 4.6) are qualitatively evaluated to understand
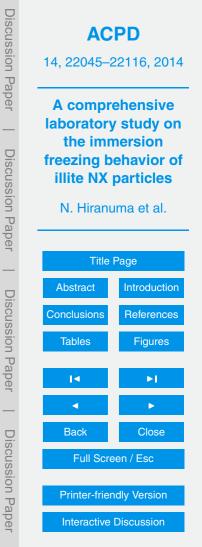
the measurement uncertainties of such techniques. Some factors may introduce diversity in n_s, whereas others may shift activation temperatures (perhaps biasing the overall accuracy and precision of instruments). Here we address the relative importance of those factors with respect to their effect on the estimation of n_s.

4.1 T-binned $n_s(T)$ analysis

Figure 7 shows the multiple exponential distribution fits (also known as the Gumbel cumulative distribution function) for T-binned data. The fits for T-binned maxima and minima n_s from seventeen measurement techniques are presented as pink shaded areas. All fits presented in this figure are derived using parameters shown in Table 3. As can be inferred from the table, a higher correlation coefficient (r) was found when intercomparing the suspension measurements as compared with the dry-dispersed methods, suggesting reasonable agreement and consistency for the results from immersion freezing studies with suspensions. Interestingly, the higher r for $n_{s,geo}$ than $n_{s,BET}$ was found for dry-dispersed particle measurements. The use of more conversion factors to estimate $n_{s,BET}$ (i.e., from Eqs. 3 and 4) may introduce uncertainties and discrepancies between measurement techniques. It is also noteworthy that the T-binned ensemble maximum and minimum values are largely influenced by dry-dispersed particle and suspension results, respectively, implying the discrepancy between two subsets (dry and suspension measurements).

It was observed that the deviation between maxima and minima in the horizontal and vertical axs (corresponding to $Hor_{Max-Min}$ and $Ver_{Max-Min}$, respectively, shown in Fig. 7) is relatively smaller for $n_{s,BET}$ compared to that for the $n_{s,geo}$. Perhaps, the use of a single BET-SSA value ($124.4\,m^2\,g^{-1}$) reduced variations in $n_{s,BET}$. Nevertheless, $n_{s,BET}$ is especially representative of measurements with suspended samples because less corrections are involved for its estimation when compared to that with dry-dispersed particles. Hence, $n_{s,BET}$ may be a good proxy for comparing IN efficiencies of dust particles from various instruments. We also report the values of $\Delta log(n_s)/\Delta T$ for four

T-segregated segments in Fig. 7 (i.e., T_1 to T_4). As expected the slope was comparable to A13 in the T_1 to T_3 segment (-11 to $-27\,°C$), while the slope in the T_4 segment is similar to N12. The largest deviations in $\text{Ver}_{\text{Max-Min}}$, corresponding to two to three orders of magnitude of n_s, were observed in a temperature region around $\sim -25\,°C$. Such high n_s variability was expected due to the contribution from MRI-DCECC, FINCH and FRIDGE measurements, which may have influenced the overall fit in that temperature range. Likewise, our $\text{Hor}_{\text{Max-Min}}$ showed that the seventeen measurements are in reasonable agreement within $6.9\,°C$ ($-34.8\,°C$, $-29.6\,°C$, $-27.9\,°C$ (min, avg, max)) at $n_{s,\text{BET}}$ of $3 \times 10^9\,\text{m}^{-2}$ and $7.4\,°C$ ($-35.7\,°C$, $-31.2\,°C$, $-28.3\,°C$ (min, avg, max)) at $n_{s,\text{geo}}$ of $10^{11}\,\text{m}^{-2}$.

Figure 8 shows T-binned $n_{s,\text{BET}}(T)$ and $n_{s,\text{geo}}(T)$ spectra in panels a and b, respectively. In this figure, panels i, ii and iii show T-binned averages of all seventeen instruments, all suspension type measurements, and all measurements that involved dry particles, respectively. We note that "EDB (contact)" and "ZINC" (Welti et al., 2009) were not used for generating T-binned data since our focus was on immersion mode freezing. We also note that the n_s results from nine IN measurement techniques provided n_s data at -23 and $-24\,°C$, where we find pronounced freezing and differences (investigated T ranges for each instrument are listed in Table 1).

As described in Sect. 3.2, suspension measurements possessed sensitivity at high temperatures (up to $-11\,°C$), indicating that their ability to control the concentration (or dilution) of suspension over a wide range is of great advantage in detecting rare INPs (sometimes one in a million particles). In turn, dry-dispersed particle measurements were advantageous for their capacity to work on a particle by particle basis and can readily explore particle size dependencies. Further, these measurements were good in general for low temperature measurements, where the number of particles nucleating ice increases and instruments have higher ice detection efficiencies. For temperatures below $-26\,°C$, our T-binned fits exhibited a reasonable agreement with the suspension experiments reported by Broadley et al. (2012). Furthermore, dry-dispersed particle measurements showed a higher freezing efficiency when compared to suspension

measurements (Fig. 8 Panel iv). We will discuss possible explanations for observed diversity of data from different techniques in detail below.

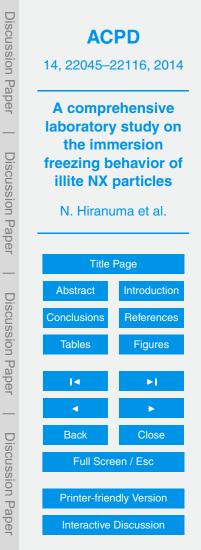## 4.2 Limitations of instrument types

As described in Sect. 3, diverse operating principles are used to measure INP characteristics. However, since there is, as yet, no absolute standard technique for intercomparison, current approaches to understand global INP distributions do not consider performance variability of IN measurement techniques. Further, there is currently no comprehensive way of representing all systematic errors in a relatively simple way rather than by relative comparison to an average (as demonstrated in Sects. 3.2 and 3.3) or by listing individual errors. Therefore, our current knowledge on the influence of systematic uncertainty upon quantitative n_s estimation is inadequate.

Groups participating in this study used different experimental setups to measure immersion freezing efficiencies of illite NX test samples. As a consequence, various experimental procedures, such as particle generation, particle size-segregation, S_{total} estimation, ice crystal detection or counting, ice crystal detection size limits for OPCs or CCDs, and particle loss at the inlet and/or in the chamber can potentially yield substantial systematic uncertainties in the estimation of n_s. Below we qualitatively discuss potential errors and limitations involved in each instrument-type (cold stage, levitator, CECC and CFDC).

Limitations of substrate-supported optical microscopy and cold stage experimental setups may come from inhomogeneous cooling of the substrate and the surrounding media, the effects of RH changes surrounding the drops, as well as potential contamination during sample preparation and measurements (e.g., particle processing in a solvent) or uncontrollable heat transfer between cold plate surface and the particle substrate (e.g., FRIDGE).

Additionally, levitator techniques require extensive pre-characterization of physico-chemical properties. Furthermore, since the overall system characterization is more
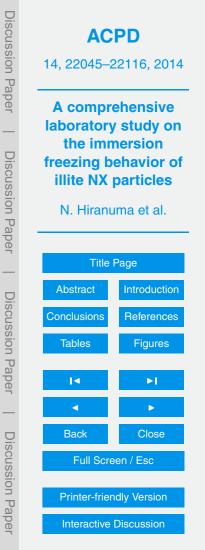
complex and labor intensive, only specific subsets (i.e., suspended samples or reference particles) can be examined using this method.

The development of AIDA-CECC allows the simulation of atmospherically representative cloud parcel formation and evolution (Möhler et al., 2003). Therefore, it is an advantage of CECC that the parameterization derived from its experiments can be most readily extended to atmospheric conditions (Niemand et al., 2012). Development of large (up to 84 m^3, i.e., AIDA) and/or temperature-controlled dynamic cloud simulation chambers (e.g., MRI-DCECC; Tajiri et al., 2013, a design which follows from DeMott and Rogers, 1990) enabled the exploration of heterogeneous ice nucleation properties of typical particulate samples in a wide range of particle concentrations, temperatures ($-100\,°C < T < 0\,°C$), cooling rates and nucleation times. However, the utilization of such an instrument to correctly measure the totality of INPs with a reasonable detection sensitivity ($< 0.1\,L^{-1}$), both in the lab and field settings, has not yet been realized due to CECC's limitations. These limitations include ice losses by settling (e.g., DeMott and Rogers, 1990) over the relatively long expansion periods in the confined vessel and internal turbulence during the expansion leading to heterogeneously supersaturated water vapor and temperature fields. These artifacts can bias IN measurements.

CFDCs are the most widely used technique to measure INPs in the atmosphere, but their inability to quantify INPs at high temperatures is an issue that exists due to the physical principals of operation, the limited sample volume (typically 1 to 2 liters per minute), and to control of the conditions leading to background frost formation in the chamber over periods of operation. Based on the operational equations in Rogers(1988), the warmest operating temperature of a CFDC is approximately −6.5 °C, controlled by the fact that the warmest wall cannot exceed 0 °C. Low sample volumes necessitate integration over longer sample periods and a general lower limit of 0.2 per liter of sampled air, absent any particle pre-concentration (Prenni et al., 2009). According to Tobo et al. (2013), the highest temperature that can be achieved in a CFDC is −9 °C. Above this threshold, temperature and ice saturation conditions cannot be maintained in the chamber. Rogers et al. (2001) and other papers since have identi-
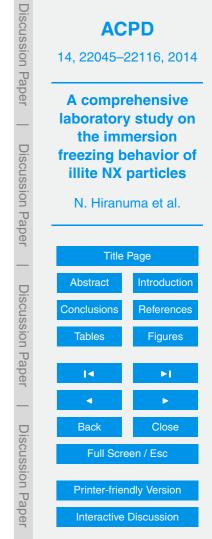
fied measurement issues due to frost emanating from the walls of the chamber when the dew point temperature of the sample air is not effectively controlled, although this appears to be an operational issue that can be mitigated if monitored properly, and will be most obtrusive for atmospheric sampling scenarios.

4.3 Stochastic nature of freezing and time-dependence

The longstanding discussion of the stochastic theory (i.e., the freezing process is time-dependent) vs. the deterministic approximation (i.e., freezing occurs at specific temperature and humidity conditions) of heterogeneous freezing has introduced another complication towards complete understanding of heterogeneous ice nucleation in the atmosphere (Vali, 2014). Many studies have attempted to characterize ice nucleation based on the classical nucleation theory (CNT), which incorporates a nucleation rate (Murray et al., 2012; Kashchiev, 2000; Mullin, 2001). In this treatment, the ice nucleation process is always of a stochastic nature (i.e., time-dependent; Bigg, 1953; Vali, 1994, 2014). According to the nucleation rate approach, the heterogeneous ice nucleation rate is strongly sensitive to INP size and the kinetic activation energy of the ice embryo on the nucleating site/surface at a specific temperature (Khvorostyanov and Curry, 2000; Fletcher, 1962). A few variants of the CNT-based approaches have been developed over the past few decades. These approaches assume uniform surface characteristics and only one ice nucleation probability (i.e., a single contact angle), nominally categorized as the single component nucleation rate approach (e.g., Bigg, 1953). Several recent studies have applied a probability density function (PDF) of contact angles and active sites over the INP surface in CNT or otherwise described a distribution of nucleation efficiencies, bridging the gap between the stochastic theory and the deterministic treatment (Marcolli et al., 2007; Lüönd et al., 2010; Kulkarni et al., 2012; Niedemeier et al., 2011; Wright and Petters., 2013; Broadley et al., 2012).

The deterministic (or time-independent) singular approximation has been developed as an alternative option to quantitatively understand atmospheric ice nucleation. The concept was first developed by Levine (1950), while the term "active sites" per surface

area was introduced by Fletcher (1969). More recently, Connolly et al. (2009) introduced the n_s density parameterization (see Sect. 2.4). This specific approach neglects the time-dependence of freezing, and assumes that a characteristic condition (e.g., temperature) must be met to nucleate ice. The semi-deterministic forms of the singular approach have a cooling rate-dependence incorporated (Vali, 2008; Herbert et al., 2014). Predicting ice nucleation from a singular perspective does not require a vast knowledge of particle-specific parameters (e.g., surface composition, structures, surface tension, solubility) that are particular to each ice nucleus and, therefore, enables ice nucleation parameterization to be relatively simple and efficient compared to the CNT-based approaches (Murray et al., 2011).

The assumption that the time-dependence of the freezing of droplets is of secondary importance when compared to temperature-dependence is supported by a recent modeling sensitivity study that showed that common INPs are substantially more sensitive to temperature than to time (Ervens and Feingold, 2013). Furthermore, while Broadley et al. (2012) showed that freezing by illite NX is time-dependent through isothermal experiments, the shift in freezing temperature on changing cooling rates by an order of magnitude was less than 0.6 °C (i.e. within the experimental uncertainty). A similar observation of weak time-dependence of immersion freezing for various types of suspended samples, inferred by comparing the results with varied cooling rate from 0.01 to 1 °C min^{-1}, is reported by Wright et al. (2013).

In the context of dry-dispersed measurements, the sensitivity of the ice nucleation to a possible time-dependence, and the respective influence on n_s, was examined to further discern its importance and uncertainty. Specifically, a contact angle distribution optimized for LACIS measurements was used to simulate the effect of a residence time varying over four orders of magnitude (i.e., 1, 10, 100 and 1000 s residence time) on n_s.

Figure 9 presents $n_s(T)$ spectra derived from modeling. To obtain them, frozen fractions for 500 nm diameter illite NX particles were calculated based on the soccer ball model (SBM; Niedermeier et al., 2011, 2014). For that, a contact angle distribution was

A comprehensive laboratory study on the immersion freezing behavior of illite NX particles

N. Hiranuma et al.

Title Page

Abstract	Introduction
Conclusions	References
Tables	Figures

|◄ | ►|

◄ | ►

Back | Close

Full Screen / Esc

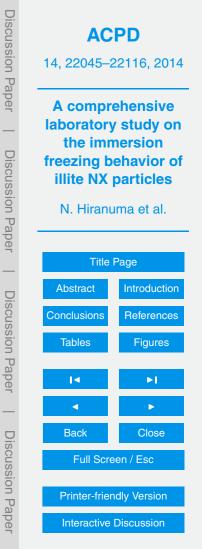Printer-friendly Version

Interactive Discussion

used which was derived based on LACIS data for the illite NX particles as shown in this work, resulting in values of 1.90 rad for the mean and 0.27 rad for the width of the contact angle distribution. Frozen fractions were obtained for ice nucleation residence times of 1, 10, 100 and 1000 s. From these, $n_{s,geo}$ was derived. An increase in the ice nucleation time by a factor of 10 resulted in a shift of approximately 1 °C towards higher freezing temperatures. This is similar to the results found in a previous study by Welti et al. (2012) for measurements of kaolinite-rich clay minerals. Indeed, $n_{s,geo}$ data obtained from AIDA agree within the measurement uncertainty with LACIS data without accounting for time-dependence. These results suggest that time-dependence of immersion freezing for illite NX particles could be neglected as a factor in the comparisons shown in Figs. 4, 5 and 6. They also imply that the immersion freezing nature of illite NX is only slightly dependent on cooling rate across a wider range of temperatures (as compared to a −26 to −37 °C as shown in Broadley et al., 2012), regardless of the sample preparation process.

4.4 Potential effect of agglomerates

As seen in the particle size distributions (Fig. 2) and agglomerated-fractions based on a relative comparison to D_{95}, aggregates are rather persistent and dominant for most of the dry-dispersed particle measurements. Since dry aggregates can have large "supermicron" sizes, they may have different IN propensities and efficiencies as compared to the sizes investigated in the present study (i.e., up to 1000 nm from PINC). Further, the degree of agglomeration may conceivably affect the surface area exposed to liquid water when suspended in supercooled droplets. Hence, an overall quantification of the effect of agglomerates is difficult. Moreover, the degree of agglomeration seems to vary from experiment to experiment, introducing diversity on the estimation of S_{total} of particles and n_s for dry-dispersed particle measurements. For instance, a combination of several methods for particle dispersion and subsequent particle size selection was employed for particle generation from illite NX samples. Further, most of the dry dispersion techniques used upstream impactors to filter out large agglomerated particles
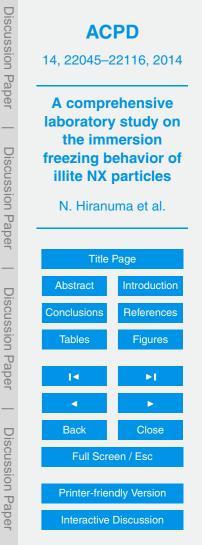
and safeguard against counting these large particles as INPs. Different types of dispersion method, impactor and size segregating instrument used in the present work are listed in the Supplement Table S1. These different aerosol generation processes may have caused different degrees of agglomeration. This may perhaps in part explain why n_s measurements obtained using dry dispersion techniques deviate from suspension measurements. Further quantification of influences of different methods for particle dispersion, size-segregation and particle impaction/filtration on the estimation of S_{total} and n_s is an important topic for future works.

In contrast, in suspension experiments, illite NX samples were directly suspended in water. Despite no pre-treatments (e.g., pre-impaction, size segregation), suspended particles appeared adequately de-agglomerated (Fig. 2a). Though the number of immersed particles can vary from droplet to droplet and the random placement of particles in the drop may be of an effect on the n_s values, the n_s spectra from suspension measurements are in general in reasonable agreement even over a wide range of wt% of illite NX samples (Fig. 6 and 8). Thus, the influence of the random placement of particles in the drop and agglomeration on the n_s estimation for suspension measurements seems small. To support this, Wright and Petters (2013) and Hader et al. (2014) simulated the role of statistical distribution in drops. The authors demonstrated that the random component due to drop placement seems to be small relative to the statistical variation due to nucleation probability. Hence, assuming the degree of agglomeration or flocculation is similar in all suspension samples, the degree of agglomeration and the random placement of particles in the drop may lead to less pronounced deviations in n_s when compared to dry-dispersed measurements.

4.5 Nucleation mode-dependence

While all suspension methods only measured immersion mode freezing of the illite NX particles, a contribution of other nucleation or freezing modes cannot be ruled out for dry-dispersed particle measurements. Hence, we now discuss inferences in the present experiments regarding the mode-dependency of the ice nucleation ability of
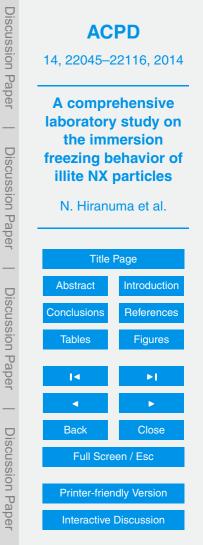
illite NX particles. Figure 10a and b shows the comparison of n_s derived from the two different operation types of FRIDGE measurements (i.e., "default mode" considers deposition mode nucleation and immersion mode freezing of dry particles in which RH_w is scanned upwards and 'imm.mode' counts immersion freezing of suspended particles in which the particles are first washed into droplets and then placed on the substrate). We investigated the ice nucleation ability of both dry and droplet suspended particles deposited on a substrate (see Supplementary Method). FRIDGE scans RH_{ice} and RH_w (low to high) at a constant temperature. During such scans we observed an abrupt increase in an activated ice fraction near water saturation as well as the highest N_{ice}, and we presumably consider ice crystals formed at the highest RH_w (near 100 % RH_w) as a measure of immersion N_{ice} from dry-dispersed particle measurements in this study.

Some default runs of FRIDGE showed much higher $n_{s,BET}$ values compared to the immersion mode runs. This difference may be a consequence of the different IN efficiencies of nucleation-modes (deposition + immersion vs. immersion alone) in the examined temperature range ($-25\,°C < T < -18\,°C$), of the different sample preparation processes (dry or suspended sample), effects of agglomeration or a combination of the three. We note that a major difference between the two measurement setups is the pressure within the instrument. For instance, default conditions involve processing at a few hPa of water vapor while the immersion measurements are conducted at atmospheric pressure. We also note that corrective post-analysis of droplet/ice separation was taken into account in this study, so that errors from counting large droplets as ice crystals were successfully removed. Interestingly, our comparison suggests that n_s derived from FRIDGE default mode seem similar to that from MRI-DCECC, in which experiments were carried out with a high degree of particle agglomeration (Fig. 2c and d).

Some other variations on applied methods suggest nucleation mode effects on the IN efficiency of illite NX particles at lower temperatures (Fig. 10c and d). For instance, the comparison between ZINC and IMCA-ZINC showed about an order of magnitude
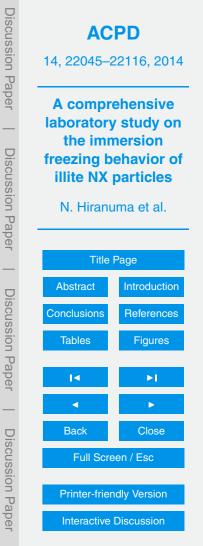
diversity in $n_{s,BET}$ beyond experimental uncertainties at −33 °C, suggesting a mode-dependent IN efficiency of clay minerals at temperatures below −25 °C. This observation is consistent with a statement that the immersion freezing parameterization from CNT may not reliably predict the activated fraction observed at $RH_w > 100\%$ as observed from condensation freezing (Welti et al., 2014). However, this is in contrast to observations indicated by PNNL-CIC below −25 °C and to results presented in Wex et al. (2014), where $n_{s,geo}$ obtained from kaolinite measurements made with LACIS and the CSU-CFDC (at $104\% > RH_w > 106\%$ for the latter) were well in agreement. When a freezing point depression was taken into account, even data obtained with the CSU-CFDC for water-vapor sub-saturated conditions was in agreement with data obtained from both, LACIS and CSU-CFDC, at water-vapor super-saturated conditions. Concerning data presented herein, PNNL-CIC and IMCA-ZINC both of which measured condensation/immersion and purely immersion mode freezing efficiency of particles, respectively, are in reasonable agreement within experimental uncertainties (Fig. 10c and d). Thus, the observed inconsistencies between methods should be subject to further methodological improvements to provide accurate data as a basis for model parameterization. Similar heterogeneous ice nucleation mode-dependent observations were made by our EDB experiments. We observed that n_s values derived from contact freezing experiments were higher than those derived from immersion ones (Fig. 10c and d).

4.6 Effect of mineralogical properties: which component of illite NX nucleates ice?

Atkinson et al. (2013) suggested that the mass fraction of K-feldspar in a sample can be used as a scaling factor to estimate n_s of other K-feldspar containing dust and soil samples. O'Sullivan et al. (2014) showed that this scaling rule could be used as an approximate predictor the n_s of soil samples once the biological ice nucleating particles were deactivated. However, inspection of Fig. 6 reveals that the line based on 14 %
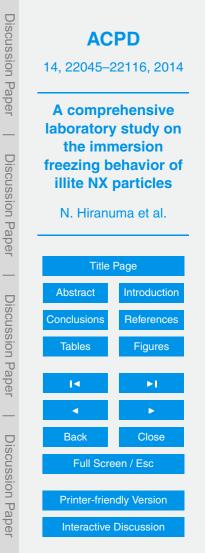
feldspar (assuming all microcline) significantly over predicts the n_s values for illite NX. There are a number of reasons why this might be.

The K-feldspar sample used by Atkinson et al. (2013) was the British Chemical Standard Chemical Reference Material (BCS-CRM) number 376/1 and X-ray diffraction analysis shows that the crystal structure is consistent with that of microcline. Microcline is one possible form of a K-feldspar and as discussed above, other K-feldspars are sanidine and orthoclase which have distinct crystal structures. The ice nucleation ability of sanidine and orthoclase are not yet published, but given they have different crystal structures they may have different nucleating abilities. Unfortunately, the X-ray diffraction analysis of illite NX is unable to identify the K-feldspar(s) present in illite NX, although the minerological analysis conducted as part of this study concluded that there was no detectable microcline in illite NX. Hence, one explanation for the K-feldspar scaling rule not working for illite NX is that there is only a trace of the strongly ice active microcline present in illite NX. For suspension measurements, only 0.0014 % microcline in illite NX reproduces the slope and magnitude of the data in Fig. 6, but this quantity of microcline is well below the detection limit of the X-ray diffraction technique. Perhaps, in the case of illite NX, it may not be the feldspar which triggers nucleation, but instead it could be another mineral present in this sample. For example, Atkinson et al. (2013) found that a quartz sample nucleated ice more efficiently than the clay minerals, but less efficiently than the feldspar samples they used. At about −28 °C, they report an n_s of $\sim 10^{10}\,\mathrm{m^{-2}}$. The X-ray analysis revealed the presence of 3 % quartz, hence we would predict an n_s of $3 \times 10^8\,\mathrm{m^{-2}}$, which is consistent with the illite NX data. Finally, an alternative explanation is that the surface of K-feldspars are chemically altered in illite NX. The surface of feldspars is known to transform to an amorphous silicate which can then recrystallize as a clay, if exposed to an acidic environment. Wex et al. (2014) suggested that it was the acid processing of K-feldspar which deactivated kaolinite samples. It is feasible that the surface of feldspar grains in illite NX have at some point become deactivated.

Title Page

Abstract	Introduction
Conclusions	References
Tables	Figures

|◄ | ►|

◄ | ►

Back | Close

Full Screen / Esc

Printer-friendly Version
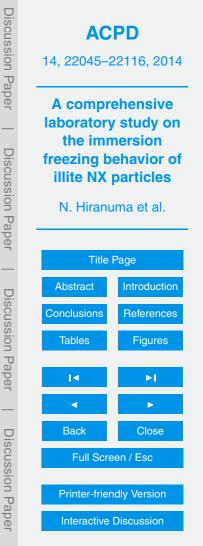
Interactive Discussion

Recently, re-partitioning of soluble components of both swelling and non-swelling clay minerals and their effect on cloud condensation nucleation activity was reported (Sullivan et al., 2010; Kumar et al., 2011; Garimella et al., 2014). To address a potential importance of this effect on the ice nucleating activity of illite NX in the wet dispersion experiments we have measured the concentration of cations released by the illite NX sample placed into deionized water as a function of time, as described in Sect. 3.1.

It is instructive to compare the amount of cations released by illite NX into aqueous environment with the value of Cation Exchange Capacity (CEC) for illite, which is known to be 25 to 40 cmol kg^{-1}(Meunier and Velde, 2004). The CEC is defined as the amount of cations retained by all the negative charges in 100 g of clay immersed in water at pH 7 (e.g., see Meunier, 2005). Per definition, CEC describes the total quantity of exchangeable cations, including interlayer cations which are in fact not accessible for substitution in non-swelling clays. The molar fraction of external cations, located on the basal planes of the crystals and on the crystal edges is roughly evaluated for illites as 20 % of the total CEC, yielding 5 to 8 cmol kg^{-1}(Wilson, 2013). Remarkably, the total amount of all cations (K^+, Na^+, Mg^{2+} and Ca^{2+}) released within the first hour by illite NX, if recalculated with account for cation valence and for the actual mass of illite in the aqueous suspension (0.1 g), gives the number 7.5 cmol kg^{-1}, which corresponds nicely with the upper bound of the external CEC (8 cmol kg^{-1}). Furthermore, Grim (1953) has shown that CEC of illite increases with decreasing size of the clay particle size, with the upper bound (~ 40 cmol kg^{-1}) being characteristic for illite with a particle size below 100 nm. This is again consistent with the very small size of particles in illite NX.

These findings have two potential implications for the measurements of illite ice nucleating efficiency obtained with different instruments. First, in the methods where dry illite particles are activated to droplets prior to cooling, the concentration of cations released into water is still far from the equilibrium and is the function of the residence time (e.g., 2–3 s for LACIS, ~ 4 s for PINC, ~ 12 s for PNNL-CIC, and over the range of several tens of seconds to a few minutes for AIDA depending on initial chamber T and RH). At the same time, the amount of external cations retained on the surface of illite parti-

cles determine the charge properties, such as charge distribution landscape and zero charge point. A potential importance of surface charge of hematite particles for their IN activity was suggested recently in Hiranuma et al. (2014b). These considerations, however speculative, might shed some light on the observed scattering of experimentally measured values of n_s. Second, for the freezing measurements where illite sample was suspended in water prior to cooling, all accessible external cations are already released into aqueous environment. In these cases the concentration of cations in the droplets is the function of mass concentration of illite in suspension. To access small supercooling temperatures, high concentrations of illite are needed in the droplet assay techniques, resulting in the possibility that not all cations are released into solution due to the inhibition of ion exchange process. Again, this would change the surface charge distribution and potentially affect the ice nucleating efficiency of illite particles. If wet particle generation (dispersion of aqueous suspension by means of a pressurized air atomizer) is used, the redistribution of cations between suspended particles may be an issue, as suggested by (Garimella et al., 2014) for the case of CCN experiments. Further studies of samples without modification or ageing after dry dispersion or wet suspension are needed to get a better idea of the method inter-comparison.

5 Conclusion

The framework of the present work is designed to advance the existing state of knowledge regarding IN measurement techniques. After ICIS-2007, there has been an increase in new instrument development, especially off-line, substrate-supported cold stage techniques, and modifications of existing online techniques. Concepts to formulate area-scaled IN efficiency with n_s parameters have also since been introduced to the community. These improvements are comprehensively evaluated in this work.

The partners of the INUIT group and external partners have for the first time identified and shared a reference mineral dust sample (illite NX) in order to get a comprehensive dataset for evaluating immersion freezing properties of atmospherically relevant parti-

cles across a wide range of particle concentrations, temperatures, cooling rates and nucleation times. Subsequently, we also compared the different laboratory methods. Illite NX samples were extensively characterized for their physico-chemical properties before they were distributed to INUIT partners and collaborators. Both bulk and single particle elemental composition analyses were conducted by XRD and EDX analyses, respectively.
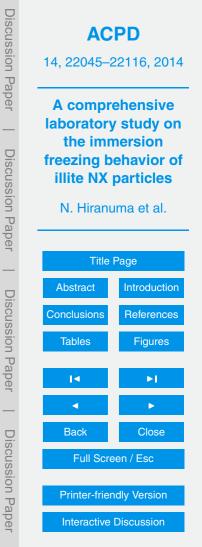
A total of seventeen IN measurement techniques were inter-compared based on their immersion freezing measurements. Our inter-comparison exercise provided unique results that would not have been achieved by individual investigators in isolation. Both consistencies and discrepancies among the instruments have been identified. Our results suggest that the immersion freezing efficiency (i.e., n_s) of illite-rich clay minerals is relatively independent of droplet size, mass percent of illite NX sample in droplets for the methods examining suspensions, physical size of illite NX particles for the methods examining dry-dispersed particles and cooling rate during freezing (within typical experimental uncertainties), verifying the premise of the n_s concept (i.e., uniform distribution of active sites for available S_{total}, strong temperature-dependency and weak time-dependency of immersion freezing for illite rich clay mineral particles).

Furthermore, comparisons of the suspension subsets against the dry-dispersed particle techniques were performed. Dry samples alone showed more diversity compared to the pre-suspended samples. This unique observation in the measurements with dry-dispersed particles may be due to the diverse methods employed for S_{total} estimation and associated uncertainties and the involvement of more active nucleation modes than just the immersion mode as compared to the suspension methods. Observed diversity in INP activity was especially pronounced at temperatures higher than about $-27\,°C$. A possible explanation for this deviation (i.e., n_s from dry-dispersed methods $> n_s$ from suspension methods) may be the chemical modification of the illite NX particles due to ion dissolution effects in the aqueous suspension.
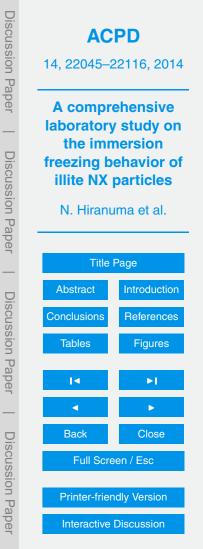
Comparisons of $\Delta \log(n_s) / \Delta T$ as an ice activation parameter suggest that the predominant freezing sites of illite NX particles exist in a temperature range between -20

and −27 °C (for suspension experiments). In comparison to the previous measurements, our synergetic work, which covers a wide temperature range, shows a similar result to the Broadley parameterization (B12), and our overall fit for the low temperature region (below −27 °C) also agrees with the Niemand parameterization (N12).

Overall accuracy and precision of IN measurement techniques was examined by evaluating T-binned (i.e., 1 °C bins) $n_s(T)$ data derived from all seventeen instruments for the temperature range from −11 to −37 °C. Our analysis revealed that discrepancies among measurements were within about 7 °C in terms of temperature and up to three orders of magnitude with respect to n_s. This diversity is much larger than the individual uncertainties of each instrument, suggesting that all instruments may be reasonably precise but it is still difficult to find overall accuracy of current IN measurement techniques, at least using illite NX as the standard and allowing partners to disperse it independently. In addition, two different n_s metrics, $n_{s,geo}$ and $n_{s,BET}$, were also compared, and we found that $n_{s,BET}$ is a better proxy for inter-comparison of the IN measurements (i.e., smaller deviation for multiple instruments).

Other than the inter-comparison aspects described above, several important implications were inferred from our study and enhanced our basic knowledge of immersion freezing. First, the existence of only a comparably small contribution of time-dependence to the inter-comparison was reconciled by the SBM. A change of the residence time, from 1 s to 10 s, shifts n_s values towards higher temperatures by only about 1 °C. Second, several nucleation modes and their contribution to nucleation efficiency were also evaluated. A comparison among EDB, ZINC and IMCA-ZINC below −25 °C implied some mode-dependencies. Likewise, a mode-dependency was also pronounced based on FRIDGE results above −25 °C. Third, immersion freezing experiments were performed with both polydisperse and size-selected illite NX particles, and size-independence of n_s for immersion freezing of "submicron" illite NX particles was also demonstrated. Finally, and most importantly, we demonstrated that a temperature change is the major driver of immersion freezing of illite NX particles. For instance, clay minerals may contain various freezing activation energies, which correspond to a wide

range of temperatures. Thus, the immersion freezing nature of clay minerals (e.g., illite NX) in a wide range of temperatures cannot be fitted by simple exponential functions but are governed by a hybrid of multi-exponential functions (a combination of scaled A13 and N12 parameterizations).

Though we shared identical test samples with each other, it is still difficult to compare n_s results because sample preparation techniques and measurement methods (e.g., particle dispersion and size distribution characterization) differ from group to group, which can result in different degrees of agglomeration or different nucleation modes (e.g., surface condensation freezing). Therefore, a continued investigation to obtain further insights of consistencies or diversity of IN measurement techniques from an experimental perspective is important to explore freezing conditions for specific compositions and more atmospherically relevant particles (e.g., soil dusts, long range transported weathered dusts, etc.). In parallel, an empirically constrained model including parameterizations of immersion freezing that correctly and efficiently represent particle-specific experimental data is also in high demand for overall predictions of current and future climate. We demonstrated that the n_s approach warrants temperature-dependent ice formation offering simplified expressions that quantitatively parameterize immersion freezing. Further developments of more simplified (efficient but accurate) descriptions, constrained by more accurate IN counting techniques, of governing atmospheric IN processes are needed.

Author contribution. J. Curtius and O. Möhler proposed the framework of this collaborative multi-institutional laboratory work. The overall manuscript, coordinated and led by N. Hiranuma, was a collaborative effort of the partners of the INUIT group and external partners. C. Budke and T. Koop designed and conducted the BINARY experiments and analyzed the data, and C. Budke contributed to the BINARY text. T. C. J. Hill carried out the CSU-IS measurements, analyzed the data, and contributed to the CSU-IS text. B. J. Murray, D. O'Sullivan and T. F. Whale performed the Leeds-NIPI experiments, analyzed the data, and contributed to the Leeds-NIPI text. K. Diehl performed the experiments and data analysis of M-AL and W-WT, and K. Diehl also contributed to their method summary text. J. D. Hader performed the NC State-CS experiments and analyzed the data, T. P. Whale contributed the analysis software, M. D. Petters

Title Page

Abstract	Introduction
Conclusions	References
Tables	Figures

|◄ | ►|

◄ | ►

Back | Close

Full Screen / Esc

Printer-friendly Version

Interactive Discussion

designed the experiments, and J. D. Hader and M. D. Petters contributed to the NC State-CS text. G. P. Schill and M. A. Tolbert conducted the CU-RMCS experiments, analyzed the data, and contributed to the CU-RMCS text. N. Hiranuma and O. Möhler conceived the AIDA experiments, analyzed and discussed the results and contributed to the AIDA text. P. J. DeMott, E. J. T. Levin and C. S. McCluskey performed CSU-CFDC experiments, analyzed the data, and contributed to the CSU-CFDC text. N. Hoffmann and A. Kiselev carried out the EDB measurements with input on experimental techniques from T. Leisner and SEM measurements and contributed to the associated data analysis and text. Björn Nillius and Fabian Frank performed the FINCH experiments and analyzed the data, and D. Rose contributed to the FINCH uncertainty analysis and method summary text. A. Danielczok and H. Bingemer conducted the FRIDGE experiments, analyzed the data, and contributed to the FRIDGE text. S. Augustin-Bauditz did the LACIS experiments, D. Niedermeier derived contact angle distributions with SBM, and H. Wex performed SBM calculations and contributed to the LACIS text. M. Murakami, K. Yamashita, T. Tajiri and A. Saito designed and performed the MRI-DCECC experiments with assistance and contributions from N. Hiranuma and O. Möhler, K. Yamashita and N. Hiranuma analyzed the MRI-DCECC data, and K. Yamashita contributed to the method summary text. Z.A. Kanji conducted the PINC experiments, Y. Boose analyzed the data, Y. Boose and Z.A. Kanji interpreted and discussed the PINC data, and contributed to the PINC text. G. Kulkarni carried out the PNNL-CIC measurements, analyzed the data, and contributed to the PNNL-CIC text. A. Welti performed the IMCA-ZINC experiments, analyzed the data, and A. Welti and Z. A. Kanji contributed to the Supplement. XRD measurements and analysis of illite NX were conducted by M. Ebert, K. Kandler and S. Weinbruch, and M. Ebert contributed the XRD text. IC measurements and analysis were carried out by A. Peckhaus and A. Kiselev, and A. Kiselev contributed to the IC text. DLS measurements and analysis were performed by K. Dreischmeier, and K. Dreischmeier also contributed to the DLS text. N. Hiranuma interpreted and analyzed the compiled data and wrote the paper. A. Kiselev and B. J. Murray co-wrote Sect. 4.6 with N. Hiranuma. All authors discussed the results and contributed to the final version of manuscript.

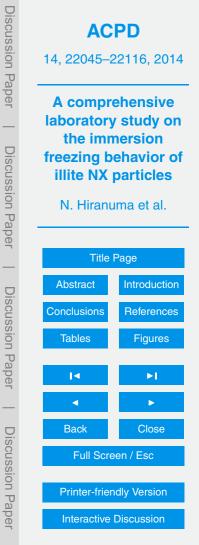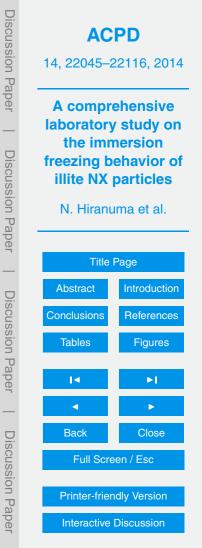**The Supplement related to this article is available online at doi:10.5194/acpd-14-22045-2014-supplement.**

References

Ardon-Dryer, K., Levin, Z., and Lawson, R. P.: Characteristics of immersion freezing nuclei at the South Pole station in Antarctica, Atmos. Chem. Phys., 11, 4015–4024, doi:10.5194/acp-11-4015-2011, 2011.

Atkinson, J. D., Murray, B. J., Woodhouse, M. T., Carslaw, K., Whale, T. F., Baustian, K., Dobbie, S., O'Sullivan, D., and Malkin, T. L.: Nature, 498, 355–358, doi:10.1038/nature12278, 2013.

Bickmore, B. R., Nagy, K. L., Sandlin, P. and Crater, T. S.: Quantifying surface areas of clays by atomic force microscopy, American Mineralogist, 87, 780–783, 2002.

Bigg, E. K.: The supercooling of water, Proc. Phys. Soc. B, 66, 688–694, doi:10.1088/0370-1301/66/8/309, 1953.

Bigg, E. K., A new technique for counting ice-forming nuclei in aerosols, Tellus, 9, 394–400, doi:10.1111/j.2153-3490.1957.tb01895.x, 1957.

Bingemer, H., Klein, H., Ebert, M., Haunold, W., Bundke, U., Herrmann, T., Kandler, K., Müller-Ebert, D., Weinbruch, S., Judt, A., Wéber, A., Nillius, B., Ardon-Dryer, K., Levin, Z., and Curtius, J.: Atmospheric ice nuclei in the Eyjafjallajökull volcanic ash plume, Atmos. Chem. Phys., 12, 857–867, doi:10.5194/acp-12-857-2012, 2012.

Boucher, O., Randall, D., Artaxo, P., Bretherton, C., Feingold, G., Forster, P., Kerminen, V.-M., Kondo, Y., Liao, H., Lohmann, U., Rasch, P., Satheesh, S. K., Sherwood, S., Stevens, B., and Zhang, X. Y.: Clouds and Aerosols. In: Climate Change 2013: The Physical Science Basis. Contribution of Working Group I to the Fifth Assessment Report of the Intergovernmental Panel on Climate Change, edited by: Stocker, T. F., Qin, D., Plattner, G.-K., Tignor, M., Allen, S. K., Boschung, J., Nauels, A., Xia, Y., Bex, V., and Midgley, P. M., Cambridge University Press, Cambridge, UK and New York, NY, USA, 2013.

Broadley, S. L., Murray, B. J., Herbert, R. J., Atkinson, J. D., Dobbie, S., Malkin, T. L., Condliffe, E., and Neve, L.: Immersion mode heterogeneous ice nucleation by an illite rich powder representative of atmospheric mineral dust, Atmos. Chem. Phys., 12, 287–307, doi:10.5194/acp-12-287-2012, 2012.

Brunauer, S., Emmett, P. H., and Teller, E.: Adsorption of gases in multimolecular layers, J. Atmos. Chem. Soc., 60, 309–319, doi:10.1021/ja01269a023, 1938.

Budke, C. and Koop, T.: BINARY: An Optical Freezing Array for Assessing Temperature and Time Dependence of Heterogeneous Ice Nucleation, Atmos. Meas. Tech. Discuss., accepted, 2014.
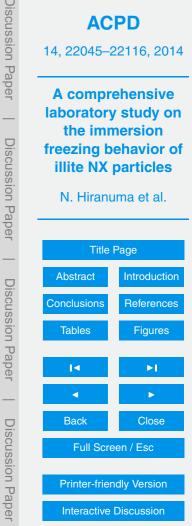
Bundke, U., Nillius, B., Jaenicke, R., Wetter, T., Klein, H., and Bingemer, H.: The fast ice nucleus chamber FINCH, Atmos. Res., 90, 180–186, doi:10.1016/j.atmosres.2008.02.008, 2008.

Chou, C., Stetzer, O.,Weingartner, E., Jurányi, Z., Kanji, Z. A., and Lohmann, U.: Ice nuclei properties within a Saharan dust event at the Jungfraujoch in the Swiss Alps, Atmos. Chem. Phys., 11, 4725–4738, doi:10.5194/acp-11-4725-2011, 2011.

Christenson, H.: Two-step crystal nucleation via capillary condensation, Cryst. Eng. Comm., 15, 2030–2039, doi:10.1039/C3CE26887J, 2013.

Connolly, P. J., Möhler, O., Field, P. R., Saathoff, H., Burgess, R., Choularton, T., and Gallagher, M.: Studies of heterogeneous freezing by three different desert dust samples, Atmos. Chem. Phys., 9, 2805–2824, doi:10.5194/acp-9-2805-2009, 2009.

Cwilong, B. M.: Sublimation centers in a Wilson chamber, Proc. Roy. Soc. A, 190, 137–143, doi:10.1098/rspa.1947.0066, 1947.

DeMott, P. J. and Rogers, D. C.: Freezing nucleation rates of dilute solution droplets measured between −30°and −40˚C in laboratory simulations of natural clouds. J. Atmos. Sci., 47, 1056–1064, doi:10.1175/1520-0469(1990)047<1056:FNRODS>2.0.CO;2, 1990.

DeMott, P. J. and Coauthors: Resurgence in ice nuclei measurement research, B. Am. Meteorol. Soc., 92, 1623–1635, doi:10.1175/2011BAMS3119.1, 2011.

DeMott, P. J., Prenni, A. J., McMeeking, G. R., Sullivan, R. C., Petters, M. D., Tobo, Y., Niemand, M., Möhler, O., Snider, J. R., Wang, Z., and Kreidenweis, S. M.: Integrating laboratory and field data to quantify the immersion freezing ice nucleation activity of mineral dust particles, Atmos. Chem. Phys. Discuss., 14, 17359–17400, doi:10.5194/acpd-14-17359-2014, 2014.

Diehl, K., Mitra, S. K., Szakáll, M., Blohn, N. v., Borrmann, S., and Pruppacher, H. R.: Chapter 2. Wind tunnels: Aerodynamics, models, and experiments. In: The Mainz vertical wind tunnel facility: A review of 25 years of laboratory experiments on cloud physics and chemistry, Pereira, J. D., Nova Science Publishers, Inc., 2011.

Diehl, K., Debertshäuser, M., Eppers, O., Schmithüsen, H., Mitra, S. K., and Borrmann, S.: Particle-area dependence of mineral dust in the immersion mode; investigations with freely suspended drops in an acoustic levitator. Atmos. Chem. Phys. Discuss., 14, 12887–12930, doi:10.5194/acpd-14-12887-2014, 2014.

Durant, A. J. and Shaw, R. A.: Evaporation freezing by contact nucleation inside-out, Geophys. Res. Lett., 32, L20814, doi:10.1029/2005GL024175, 2005.

Dymarska, M., Murray, B. J., Sun, L. M., Eastwood, M. L., Knopf, D. A., and Bertram, A. K.: Deposition ice nucleation on soot at temperatures relevant for the lower troposphere, J. Geophys. Res., 111, 2006.

Ervens, B. and Feingold, G.: Sensitivities of immersion freezing: Reconciling classical nucleation theory and deterministic expressions, Geophys. Res. Lett., 40, 3320–3324, doi:10.1002/grl.50580, 2013.

Fletcher, N. H.: Physics of Rain Clouds, Cambridge Univ. Press, New York, USA, 1962.

Fletcher, N. H.: Active sites and ice crystal nucleation, J. Atmos. Sci., 26, 6, 1266–1271, doi:10.1175/1520-0469(1969)026<1266:ASAICN>2.0.CO;2, 1969.

Fornea, A. P., Brooks, S. D., Dooley, J. B., and Saha, A. Heterogeneous freezing of ice on atmospheric aerosols containing ash, soot, and soil, J. Geophys. Res., 114, D13201, doi:10.1029/2009JD011958, 2009.

Fournier D'albe, E. M.: Some experiments on the condensation of water vapour at temperatures below 0 °C, Q. J. Roy. Meteor. Soc., 75, 1–16, doi:10.1002/qj.49707532302, 1949.

Friedman, B., Kulkarni, G., Beránek, J., Zelenyuk, A., Thornton, J. A., and Cziczo, D. J.: Ice nucleation and droplet formation by bare and coated soot particles, J. Geophys. Res., 116, D17203, doi:10.1029/2011JD015999, 2011.

Friedrich, F., Steudel, A., and Weidler, P. G.: Change of the refractive index of illite particles by reduction of the Fe content of the octahedral sheet, Clays Clay Miner., 56, 505–510, doi:10.1346/CCMN.2008.0560503, 2008.

Garimella, S., Huang, Y.-W., Seewald, J. S., and Cziczo, D. J.: Cloud condensation nucleus activity comparison of dry- and wet-generated mineral dust aerosol: the significance of soluble material, Atmos. Chem. Phys., 14, 6003–6019, doi:10.5194/acp-14-6003-2014, 2014.
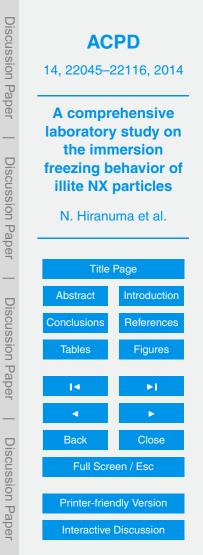
Gregg, S. L. and Sing, K. S. W.: Adsorption, surface area and porosity, Academic Press, London, UK, 303 pp., 1982.

Grim, R. E.: Clay mineralogy, McGraw-Hill, New York, USA, 384 pp., 1953.

Hader, J. D., Wright, T. P., and Petters, M. D.: Contribution of pollen to atmospheric ice nuclei concentrations, Atmos. Chem. Phys., 14, 5433–5449, doi:10.5194/acp-14-5433-2014, 2014.

Hartmann, S., Niedermeier, D., Voigtländer, J., Clauss, T., Shaw, R. A., Wex, H., Kiselev, A., and Stratmann, F.: Homogeneous and heterogeneous ice nucleation at LACIS: operating principle and theoretical studies, Atmos. Chem. Phys., 11, 1753–1767, doi:10.5194/acp-11-1753–2011, 2011.

Title Page

Abstract | Introduction

Conclusions | References

Tables | Figures

|◀ | ▶|

◀ | ▶

Back | Close

Full Screen / Esc

Printer-friendly Version

Interactive Discussion

Herbert, R. J., Murray, B. J., Whale, T. F., Dobbie, S. J., and Atkinson, J. D.: Representing time-dependent freezing behaviour in immersion mode ice nucleation, Atmos. Chem. Phys., 14, 8501–8520, doi:10.5194/acp-14-8501-2014, 2014.

Hill, T. C. J., Moffett, B. F., DeMott, P. J., Georgakopoulos, D. G., Stump, W. L., and Franc, G. D.: Measurement of Ice Nucleation-Active Bacteria on Plants and in Precipitation by Quantitative PCR, Appl. Environ. Microbiol., 80, 1256–1267, doi:10.1128/AEM.02967-13, 2014.

Hiranuma, N., Brooks, S. D., Moffet, R., Glen, A., Laskin, A., Gilles, M. K., Liu, P., MacDonald, M. A., Strapp, W., and McFarquhar, G. M.: Chemical characterization of individual particles and residuals of cloud droplets and ice crystals collected on board research aircraft in the ISDAC 2008 study, J. Geophys. Res., 118, 6564–6579, doi:10.1002/jgrd.50484, 2013.

Hiranuma, N., Paukert, M., Steinke, I., Zhang, K., Kulkarni, G., Hoose, C., Schnaiter, M., Saathoff, H., and Möhler, O.: A comprehensive parameterization of heterogeneous ice nucleation of dust surrogate: laboratory study with hematite particles and its application to atmospheric models, Atmos. Chem. Phys. Discuss., 14, 16493–16528, doi:10.5194/acpd-14-16493-2014, 2014a.
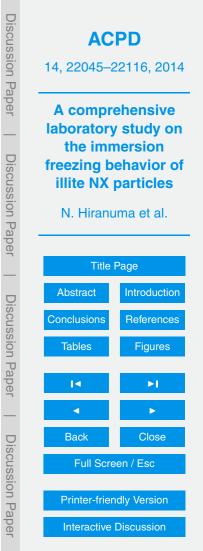
Hiranuma, N., Hoffmann, N., Kiselev, A., Dreyer, A., Zhang, K., Kulkarni, G., Koop, T., and Möhler, O.: Influence of surface morphology on the immersion mode ice nucleation efficiency of hematite particles, Atmos. Chem. Phys., 14, 2315–2324, doi:10.5194/acp-14-2315-2014, 2014b.

Hoffmann, N., Kiselev, A., Rzesanke, D., Duft, D., and Leisner, T.: Experimental quantification of contact freezing in an electrodynamic balance, Atmos. Meas. Tech., 6, 2373–2382, doi:10.5194/amt-6-2373-2013, 2013.

Hoose, C., Kristjansson, J. E., Chen, J.-P., and Hazra, A.: A classical-theory-based parameterization of heterogeneous ice nucleation by mineral dust, soot, and biological particles in a global climate model, J. Atmos. Sci., 67, 2483–2503, doi:10.1175/2010JAS3425.1, 2010.

Hoose, C. and Möhler, O.: Heterogeneous ice nucleation on atmospheric aerosols: a review of results from laboratory experiments, Atmos. Chem. Phys., 12, 9817–9854, doi:10.5194/acp-12-9817-2012, 2012.

Hussain, K. and Saunders, C. P. R.: Ice nucleus measurement with a continuous flow chamber. Q. J. Roy. Meteor. Soc., 110, 75–84, doi:10.1002/qj.49711046307, 1984.

Iannone, R., Chernoff, D. I., Pringle, A., Martin, S. T., and Bertram, A. K.: The ice nucleation ability of one of the most abundant types of fungal spores found in the atmosphere, Atmos. Chem. Phys., 11, 1191–1201, doi:10.5194/acp-11-1191-2011, 2011.

A comprehensive laboratory study on the immersion freezing behavior of illite NX particles

N. Hiranuma et al.

Title Page

Abstract | Introduction

Conclusions | References

Tables | Figures

|◀ | ▶|

◀ | ▶

Back | Close

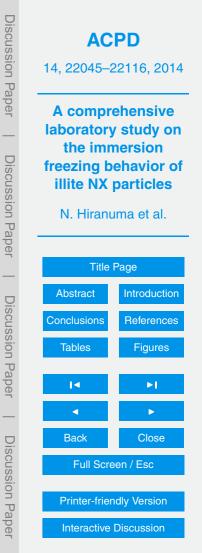Full Screen / Esc

Printer-friendly Version

Interactive Discussion

Kanji, Z. A. and Abbatt, J. P. D.: Laboratory studies of ice formation via deposition mode nucleation onto mineral dust and n-hexane soot samples, J. Geophys. Res., 111, D16204, doi:10.1029/2005JD006766, 2006.

Kanji, Z. A. and Abbatt, J. P. D.: The University of Toronto Continuous Flow Diffusion Chamber (UT-CFDC): A simple design for ice nucleation studies, Aerosol Sci. Technol., 43, 730–738. doi:10.1080/02786820902889861, 2009.

Kanji, Z. A., Welti, A., Chou, C., Stetzer, O., and Lohmann, U.: Laboratory studies of immersion and deposition mode ice nucleation of ozone aged mineral dust particles, Atmos. Chem. Phys., 13, 9097–9118, doi:10.5194/acp-13-9097-2013, 2013.

Kashchiev, D.: Nucleation: Basic Theory with Applications, Butterworth-Heinemann, Oxford, UK, 544 pp., 2000.

Khvorostyanov, V. I. and Curry, J. A.: A new theory of heterogeneous nucleation for application in cloud and climate models, Geophys. Res. Lett., 27, 4081–4084, doi:10.1029/1999GL011211, 2000.

Kline, D. B. and Brier, G. W.: Some experiments on the measurement of natural ice nuclei, Mon. Weather Rev., 89, 263–272, doi:10.1175/1520-0493(1961)089<0263:SEOTMO>2.0.CO;2, 1961.

Knopf, D. A. and Alpert, P. A.: A water activity based model of heterogeneous ice nucleation kinetics for freezing of water and aqueous solution droplets, Faraday Discuss., 165, 513–534, doi:10.1039/C3FD00035D, 2013.

Koop, T., Luo, B., Tsias, A., and Peter, T.: Water activity as the determinant for homogeneous ice nucleation in aqueous solutions, Nature, 406, 611–614, doi:10.1038/35020537, 2000.

Kulkarni, G., Fan, J., Comstock, J. M., Liu, X., and Ovchinnikov, M.: Laboratory measurements and model sensitivity studies of dust deposition ice nucleation, Atmos. Chem. Phys., 12, 7295–7308, doi:10.5194/acp-12-7295-2012, 2012.

Kumar, P., Sokolik, I. N., and Nenes, A.: Cloud condensation nuclei activity and droplet activation kinetics of wet processed regional dust samples and minerals, Atmos. Chem. Phys., 11, 8661–8676, doi:10.5194/acp-11-8661-2011, 2011.

Levine, J.: Statistical explanation of spontaneous freezing of water droplets, NACA Tech. Notes, no. 2234, 1950.

Lüönd, F., Stetzer, O., Welti, A., and Lohmann, U.: Experimental study on the ice nucleation ability of size-selected kaolinite particles in the immersion mode, J. Geophys. Res., 115, D14201, doi:10.1029/2009JD012959, 2010.

Title Page

Abstract | Introduction

Conclusions | References

Tables | Figures

◄ | ►

◄ | ►

Back | Close

Full Screen / Esc

Printer-friendly Version

Interactive Discussion

Marcolli, C., Gedamke, S., Peter, T., and Zobrist, B.: Efficiency of immersion mode ice nucleation on surrogates of mineral dust, Atmos. Chem. Phys., 7, 5081–5091, doi:10.5194/acp-7-5081-2007, 2007.

Marcolli, C.: Deposition nucleation viewed as homogeneous or immersion freezing in pores and cavities, Atmos. Chem. Phys., 14, 2071–2104, doi:10.5194/acp-14-2071-2014, 2014.

Meunier, A.: Clays, Springer, 472 pp., 2005.

Meunier, A., and Velde.: Illite: Origins, Evolution and Metamorphism, Springer, 286 pp., 2004.

Möhler, O., Stetzer, O., Schaefers, S., Linke, C., Schnaiter, M., Tiede, R., Saathoff, H., Krämer, M., Mangold, A., Budz, P., Zink, P., Schreiner, J., Mauersberger, K., Haag, W., Kärcher, B., and Schurath, U.: Experimental investigation of homogeneous freezing of sulphuric acid particles in the aerosol chamber AIDA, Atmos. Chem. Phys., 3, 211–223, doi:10.5194/acp-3-211-2003, 2003.

Mullin, J. W.: Crystallization, Elsevier Butterworth-Heinemann, Oxford, UK, Forth edn., 600 pp., 2001.

Murray, B. J., Broadley, S. L., Wilson, T. W., Bull, S. J., Wills, R. H., Christenson, H. K., and Murray, E. J.: Kinetics of the homogeneous freezing of water, Phys. Chem. Chem. Phys., 12, 10380–10387, doi:10.1039/c003297b, 2010.

Murray, B. J., Broadley, S. L., Wilson, T. W., Atkinson, J. D., and Wills, R. H.: Heterogeneous freezing of water droplets containing kaolinite particles, Atmos. Chem. Phys., 11, 4191–4207, doi:10.5194/acp-11-4191-2011, 2011.

Murray, B. J., O'Sullivan, D., Atkinson, J. D., and Webb, M. E.: Ice nucleation by particles immersed in supercooled cloud droplets, Chem. Soc. Rev., 41, 6519–6554, doi:10.1039/c2cs35200a, 2012.

Niedermeier, D., Shaw, R. A., Hartmann, S., Wex, H., Clauss, T., Voigtländer, J., and Stratmann, F.: Heterogeneous ice nucleation: exploring the transition from stochastic to singular freezing behavior, Atmos. Chem. Phys., 11, 8767–8775, doi:10.5194/acp-11-8767-2011, 2011.

Niedermeier, D., Ervens, B., Clauss, T., Voigtländer, J., Wex, H., Hartmann, S., and Stratmann, F.: A computationally efficient description of heterogeneous freezing: A simplified version of the soccer ball model, Geophys. Res. Lett., 41, 736–741, doi:10.1002/2013GL058684, 2014.

Niehaus, J, Bunker, K. W., China, S., Kostinski, A., Mazzoleni, C., Cantrell, W.: A technique to measure ice nuclei in the contact mode, J. Atmos. Oceanic Technol., 31, 913–922, doi:10.1175/JTECH-D-13-00156.1, 2014.

Niemand, M., Möhler, O., Vogel, B., Vogel, H., Hoose, C., Connolly, P., Klein, H., Bingemer, H., DeMott, P., and Skrotzki, J.: A particle-surface-area-based parameterization of immersion freezing on desert dust particles, J. Atmos. Sci., 69, 3077–3092, doi:10.1175/Jas-D-11-0249.1, 2012.

O'Sullivan, D., Murray, B. J., Malkin, T. L., Whale, T. F., Umo, N. S., Atkinson, J. D., Price, H. C., Baustian, K. J., Browse, J., and Webb, M. E.: Ice nucleation by fertile soil dusts: relative importance of mineral and biogenic components, Atmos. Chem. Phys., 14, 1853–1867, doi:10.5194/acp-14-1853-2014, 2014.

Palmer, H. P.: Natural ice-particle nuclei, Q. J. Roy. Meteorol. Soc., 75, 17–22, doi:10.1002/qj.49707532303, 1949.

Prenni, A. J., DeMott, P. J., Rogers, D. C., Kreidenweis, S. M., McFarquhar, G. M., Zhang, G., and Poellot, M. R.: Ice nuclei characteristics from M-PACE and their relation to ice formation in clouds, Tellus, 61B, doi:10.1111/j.1600-0889.2009.00415.x, 436–448. 2009.

Quantachrome Instruments: Autosorb iQ/ASiQwin Operating Manual, Sect. J. Theory and Discussion, 359–360, 2013.

Riechers, B., Wittbracht, F., Hütten, A., and Koop, T.: The homogeneous ice nucleation rate of water droplets produced in a microfluidic device and the role of temperature uncertainty, Phys. Chem. Chem. Phys., 15, 5873–5887, doi:10.1039/c3cp42437e, 2013.

Rogers, D. C.: Development of a continuous flow thermal gradient diffusion chamber for ice nucleation studies, Atmos. Res., 22, 149–181, doi:10.1016/0169-8095(88)90005-1, 1988.
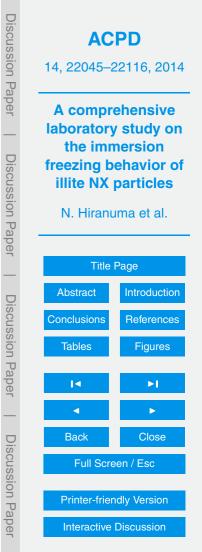
Rogers, D. C., DeMott, P. J., Kreidenweis, S. M., and Chen, Y.: A continuous-flow diffusion chamber for airborne measurements of ice nuclei, J. Atmos. Oceanic Technol., 18, 725–741, doi:10.1175/1520-0426(2001)018<0725:ACFDCF>2.0.CO;2, 2001.

Rosenfeld, D. and Woodley, W. L.: Deep convective clouds with sustained supercooled liquid water down to −37.5 °C, Nature, 405, 440–442, doi:10.1038/35013030, 2000.

Schill, G. P. and Tolbert, M. A.: Heterogeneous ice nucleation on phase-separated organic-sulfate particles: effect of liquid vs. glassy coatings, Atmos. Chem. Phys., 13, 4681–4695, doi:10.5194/acp-13-4681-2013, 2013.

Steinke, I., Möhler, O., Kiselev, A., Niemand, M., Saathoff, H., Schnaiter, M., Skrotzki, J., Hoose, C., and Leisner, T.: Ice nucleation properties of fine ash particles from the Eyjafjallajökull eruption in April 2010, Atmos. Chem. Phys., 11, 12945–12958, doi:10.5194/acp-11-12945-2011, 2011.

Title Page

Abstract | Introduction

Conclusions | References

Tables | Figures

|◄ | ►|

◄ | ►

Back | Close

Full Screen / Esc

Stetzer, O., Baschek, B., Luond, F., and Lohmann, U.: The Zurich Ice Nucleation Chamber (ZINC) – A new instrument to investigate atmospheric ice formation, Aerosol Sci. Technol., 42, 64–74, doi:10.1080/02786820701787944, 2008.

Sullivan, R. C., Moore, M. J. K., Petters, M. D., Kreidenweis, S. M., Qafoku, O., Laskin, A., Roberts, G. C., and Prather, K. A.: Impact of particle generation method on the apparent hygroscopicity of insoluble mineral particles, Aerosol Sci. Tech., 44, 830–846, 2010.

Szakáll, M., Diehl, K., Mitra, S. K., and Borrmann, S.: A wind tunnel study on the shape, oscillation, and internal circulation of large raindrops with sizes between 2.5 and 7.5 mm, J. Atmos. Sci., 66, 755–765, doi:10.1175/2008JAS2777.1, 2009.

Tajiri, T., Yamashita, K., Murakami, M., Orikasa, N., Saito, A., Kusunoki, K., and Lilie, L.: A novel adiabatic-expansion-type cloud simulation chamber, J. Meteor. Soc. Jpn., 91, 5, 687–704, doi:10.2151/jmsj.2013-509, 2013.

Tobo, Y., Prenni, A. J., DeMott, P. J., Huffman, J. A., McCluskey, C. S. , Tian,G., Pöhlker,C., Pöschl, U., and Kreidenweis, S. M.: Biological aerosol particles as a key determinant of ice nuclei populations in a forest ecosystem, J. Geophys. Res. Atmos., 118, 10100–10110, doi:10.1002/jgrd.50801, 2013.

Tomlinson, E. M. and Fukuta, N.: A new horizontal gradient, continuous flow, ice thermal diffusion chamber. J. Atmos. Oceanic Technol., 2, 448–467, doi:10.1175/1520-0426(1985)002<0448:ANHGCF>2.0.CO;2., 1985.

Vali, G.: Nucleation terminology, J. Aerosol Sci., 16, 575–576, doi:10.1016/0021-8502(85)90009-6, 1985.

Vali, G.: Freezing rate due to heterogeneous nucleation, J. Atmos. Sci., 51, 1843–1856, doi:10.1175/1520-0469(1994)051<1843:FRDTHN>2.0.CO;2, 1994.

Vali, G.: Repeatability and randomness in heterogeneous freezing nucleation, Atmos. Chem. Phys., 8, 5017–5031, doi:10.5194/acp-8-5017-2008, 2008.

Vali, G.: Interpretation of freezing nucleation experiments: singular and stochastic; sites and surfaces, Atmos. Chem. Phys., 14, 5271–5294, doi:10.5194/acp-14-5271-2014, 2014.

Veghte, D. P. and Freedman, M. A.: Facile method for determining the aspect ratios of mineral dust aerosol by electron microscopy, Aerosol Sci. Technol., 48, 715–724, doi:10.1080/02786826.2014.920484, 2014.

Wagner, R., Möhler, O., Saathoff, H., Schnaiter, M., and Leisner, T.: New cloud chamber experiments on the heterogeneous ice nucleation ability of oxalic acid in the immersion mode, Atmos. Chem. Phys., 11, 2083–2110, doi:10.5194/acp-11-2083-2011, 2011.

Waseda, Y., Matsubara, E., and Shinoda, K.: X-Ray Diffraction Crystallography: Introduction, Examples and Solved Problems, Springer, 310 pp., 2011.

Wegener, A.: Thermodynamik der Atmosphäre. J. A. Barth Verlag, 311 pp., 1911.

Welti, A., Lüönd, F., Stetzer, O., and Lohmann, U.: Influence of particle size on the ice nucleating ability of mineral dusts, Atmos. Chem. Phys., 9, 6705–6715, doi:10.5194/acp-9-6705-2009, 2009.

Welti, A., Lüönd, F., Kanji, Z. A., Stetzer, O., and Lohmann, U.: Time dependence of immersion freezing: an experimental study on size selected kaolinite particles, Atmos. Chem. Phys., 12, 9893–9907, doi:10.5194/acp-12-9893-2012, 2012.

Welti, A., Kanji, Z. A., Lüönd, F., Stetzer, O., and Lohmann, U.: Exploring the mechanisms of ice nucleation on kaolinite: from deposition nucleation to condensation freezing, J. Atmos. Sci., 71, 16–36, doi:10.1175/JAS-D-12-0252.1, 2014.

Welton, J. E.: SEM Petrology Atlas, The American Association of Petroleum Geologists, Tulsa, OK, USA, 240 pp., 1984.

Wex, H., DeMott, P. J., Tobo, Y., Hartmann, S., Rösch, M., Clauss, T., Tomsche, L., Niedermeier, D., and Stratmann, F.: Kaolinite particles as ice nuclei: learning from the use of different kaolinite samples and different coatings, Atmos. Chem. Phys., 14, 5529–5546, doi:10.5194/acp-14-5529-2014, 2014.

Wilson, M. J.: Sheet Silicates: Clay Minerals In: Rock-Forming Minerals, 3C, edited by: Deer, W. A., Howie, R. A., and Zussman, J., The Geological Society, 736 pp., 2013.

Wright, T. P. and Petters, M. D.: The role of time in heterogeneous freezing nucleation, J. Geophys. Res. Atmos., 118, 3731–3743, doi:10.1002/jgrd.50365, 2013.

Wright, T. P. and Petters, M. D.: The role of time in heterogeneous freezing nucleation, J. Geophys. Res. Atmos., 118, 3731–3743, doi:10.1002/jgrd.50365, 2013.

Wright, T. P., Petters, M. D., Hader, J. D., Morton, T., and Holder, A. L.: Minimal cooling rate dependence of ice nuclei activity in the immersion mode, J. Geophys. Res.-Atmos., 118, 1–9, doi:10.1002/jgrd.50810, 2013.

A comprehensive laboratory study on the immersion freezing behavior of illite NX particles

N. Hiranuma et al.

Table 1. Summary of INUIT measurement techniques and instruments. Their acronyms are available in the Supplementary Information. Note "poly" and "mono" denote polydisperse and quasi-monodisperse size-selected particle distributions, respectively.

ID	Instrument	Description	Mobile	Reference	Investigable T range	Investigated T range for this study
1	BINARY[*]	Cold stage-supported droplet assay	No	Budke and Koop (2014)	$-25\,°C < T < {\sim}\,0\,°C$	$-24\,°C < T < -15\,°C$
2	CSU-IS	Immersion mode ice spectrometer	Yes	Hill et al. (2014)	$-30\,°C < T < {\sim}\,0\,°C$	poly: $-25\,°C < T < -11\,°C$ mono: $-26\,°C < T < -20\,°C$
3	Leeds-NIPI	Nucleation by immersed particles instrument	No	O'Sullivan et al. (2014)	$-36\,°C < T < {\sim}\,0\,°C$	$-21\,°C < T < -11\,°C$
4	M-AL[*]	Acoustic droplet levitator	No	Diehl et al. (2014)	$-30\,°C < T < {\sim}\,0\,°C$	$-25\,°C < T < -15\,°C$
5	M-WT[*]	Vertical wind tunnel	No	Szakáll et al. (2009); Diehl et al. (2011)	$-30\,°C < T < {\sim}\,0\,°C$	$-21\,°C < T < -19\,°C$
6	NC State-CS	Cold stage-supported droplet assay	No	Wright and Petters, 2013	$-40\,°C < T < {\sim}\,0\,°C$	$-34\,°C < T < -14\,°C$
7	CU-RMCS	Cold stage-supported droplet assay	No	Schill and Tolbert, 2013	$-40\,°C < T < -20\,°C$	$-32\,°C < T < -23\,°C$
8	AIDA[*]	CECC	No	Möhler et al. (2003) Hiranuma et al. (2014a, b)	$-100\,°C < T < -5\,°C$	poly: $-35\,°C < T < -27\,°C$ mono: $-34\,°C < T < -28\,°C$
9	CSU-CFDC	Cylindrical plates CFDC	Yes	Tobo et al. (2013)	$-34\,°C < T < -9\,°C$	$-29\,°C < T < -22\,°C$
10	EDB[*]	Electrodynamic balance levitator	No	Hoffmann et al. (2013)	$-40\,°C < T < -1\,°C$	[a]imm.: $-31\,°C < T < -28\,°C$ [b] contact: $-34\,°C < T < -27\,°C$
11	FINCH[*]	Continuous flow mixing chamber	Yes	Bundke et al. (2008)	$-60\,°C < T < -2\,°C$	$-27\,°C < T < -22\,°C$
12	FRIDGE[*]	Substrate-supported diffusion and condensation/immersion cell	Yes	Bingemer et al. (2012)	$-25\,°C < T < -8\,°C$	[c] default: $-25\,°C < T < -18\,°C$ [d] imm.: $-25\,°C < T < -18\,°C$
13	LACIS[*]	Laminar flow tube	No	Hartmann et al. (2011); Wex et al. (2014)	$-40\,°C < T < -5\,°C$	$-37\,°C < T < -31\,°C$
14	MRI-DCECC	Dynamic CECC	No	Tajiri et al. (2013)	$-100\,°C < T < {\sim}\,0\,°C$	poly: $-26\,°C < T < -21\,°C$ mono: $-29\,°C < T < -21\,°C$
15	PINC	Parallel plates CFDC	Yes	Chou et al. (2011); Kanji et al. (2013)	$-40\,°C < T < -9\,°C$	$-35\,°C < T < -26\,°C$
16	PNNL-CIC	Parallel plates CFDC	Yes	Friedman et al. (2011)	$-55\,°C < T < -15\,°C$	$-35\,°C < T < -27\,°C$
17	IMCA-ZINC	Parallel plates CFDC	No	Lüönd et al. (2010) Stetzer et al. (2008); Welti et al. (2009)	$-65\,°C < T < -5\,°C$	[e]imm.: $-36\,°C < T < -31\,°C$ [f]ZINC: $-33\,°C < T < -32\,°C$

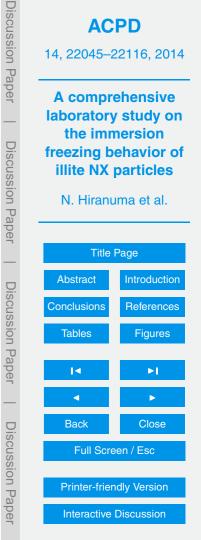[*] instruments of INUIT project partners,
[a] immersion freezing,
[b] contact freezing,
[c] default deposition nucleation,
[d] immersion freezing with suspended particles,
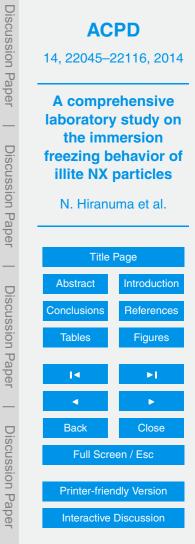[e] immersion freezing with IMCA,
[f] ZINC alone.

Table 2. X-ray diffraction analyses of the bulk composition of illite NX powder.

Mineral	Weight percentage (wt %)			
	This study	Manufacturer data	Broadley et al. (2012)	Friedrich et al. (2008)[*]
Illite	69	86	74	76
Kaolinite	10	10	7	5
Quartz	3	4	7	< 1
Calcite/carbonate	3	N/A	2	2
Feldspar (orthoclase/sanidine)	14	N/A	10	4

[*] Friedrich et al. (2008) noted 11 wt % additional impurities, including phlogopite (7.8 wt %), anhydrite (1.4 wt %), plagioclase (1.1 wt %), and apatite (0.7 wt %).

Table 3. List of the Gumbel cumulative distribution fit parameters to the $n_{s,BET}$ and $n_{s,geo}$ for T-binned ensemble dataset (All), ensemble maximum values (All$_{max}$), ensemble minimum values (All$_{min}$), suspension subset (Sus) and dry-dispersed particle subset (Dry). The correlation coefficient, r, for each fit is also shown. T is in °C.

Fitted dataset	Fitted T range	Fit parameters [$n_{s,BET}(T) = \exp(a \cdot \exp(-\exp(b \cdot (T + c))) + d)$]				
		a	b	c	d	r
All[*]	$-37\,°C < T < -11\,°C$	23.82	0.16	17.49	1.39	0.58
All$_{max}$[*]	$-37\,°C < T < -11\,°C$	24.72	0.15	17.27	1.56	0.63
All$_{min}$[*]	$-37\,°C < T < -11\,°C$	21.86	0.16	22.73	2.90	0.98
Sus	$-34\,°C < T < -11\,°C$	24.38	0.14	19.61	1.89	0.99
Dry[*]	$-37\,°C < T < -18\,°C$	27.35	0.07	16.48	3.19	0.58
Fitted dataset	Fitted T range	Fit Parameters [$n_{s,geo}(T) = \exp(a \cdot \exp(-\exp(b \cdot (T + c))) + d)$]				
		a	b	c	d	r
All[*]	$-37\,°C < T < -11\,°C$	25.75	0.13	17.17	3.34	0.74
All$_{max}$	$-37\,°C < T < -11\,°C$	25.72	0.15	16.39	3.52	0.75
All$_{min}$[*]	$-37\,°C < T < -11\,°C$	22.16	0.16	21.73	5.42	0.97
Sus	$-34\,°C < T < -11\,°C$	22.72	0.16	19.52	5.50	1.00
Dry[*]	$-37\,°C < T < -18\,°C$	29.38	0.05	16.49	7.19	0.64

[*] To derive the fits that are representative for immersion mode freezing, we excluded EDB_contact and ZINC data.
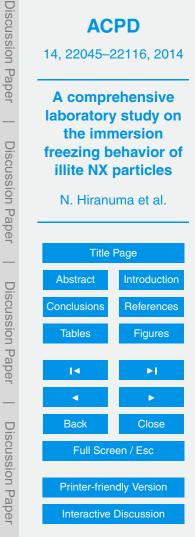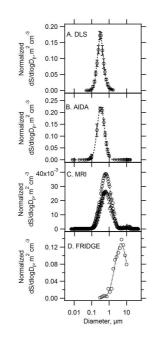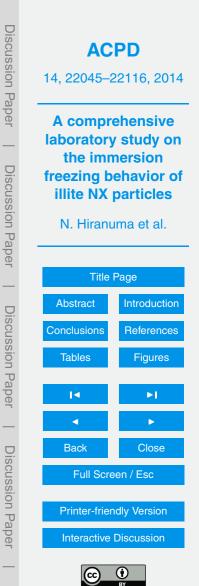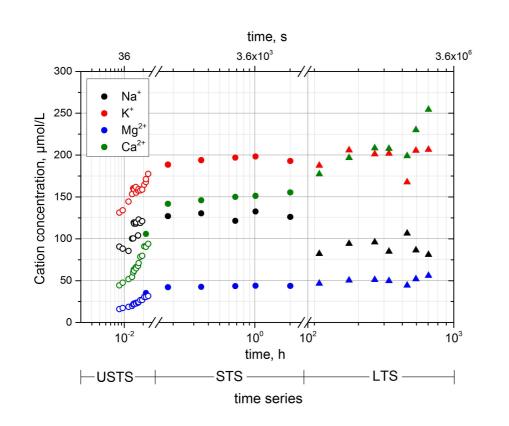
Figure 1. EDX spectra of representative illite NX particles. **(a)** typical illite, **(b)** calcite rich mineral, **(c)** titanium oxide rich mineral, and **(d)** lead rich mineral. Scanning electron microscopy images of characterized particles are shown in subpanels. Schematic representation of the illite's crystal structure (silicon in yellow, aluminum in black, oxygen in red and potassium in purple) is also shown.
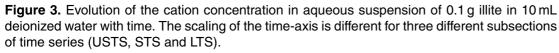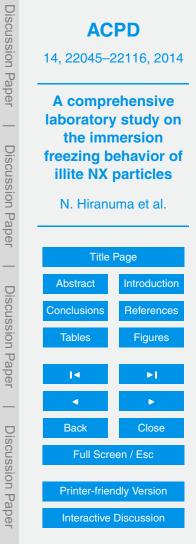
Figure 2. Surface area distributions of **(a)** suspended and **(b–d)** dry illite NX particles. Hydrodynamic size-based surface area distributions are measured in suspension using DLS. The average (± standard error) of five measurements with different concentrations of suspended illite NX powder (0.05, 0.1, 0.25, 0.5 and $1\,mg\,mL^{-1}$) is presented in **(a)**. Volume equivalent diameter-based dry-dispersed particle surface area distributions measured in the AIDA chamber (mean of ten measurements ± standard error) and MRI-DCECC (two individual measurements) are shown in **(b)** and **(c)**, respectively. **(d)** shows optical diameter-based particle surface area distributions measured by a TSI-OPS used for FRIDGE experiments. Dotted lines represent log-normal fits, and corresponding mode diameters are **(a)** 0.32 μm, **(b)** 0.33 μm, **(c)** 0.62 μm and **(d)** 4.75 μm. The width-parameters of log-normal fittings are **(a)** 0.57, **(b)** 0.69, **(c)** 0.96 and **(d)** 1.11.
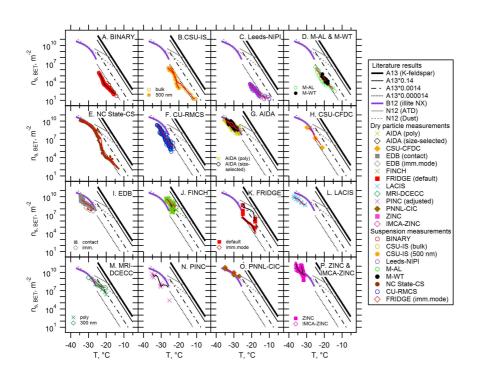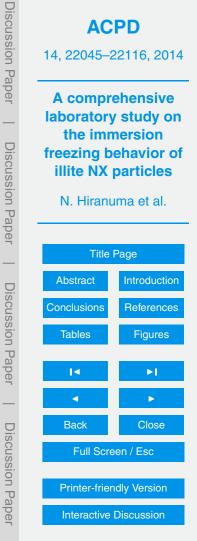
Title Page

Abstract | Introduction

Conclusions | References

Tables | Figures

|◄ | ►|

◄ | ►

Back | Close

Full Screen / Esc

Printer-friendly Version

Interactive Discussion

Figure 3. Evolution of the cation concentration in aqueous suspension of 0.1 g illite in 10 mL deionized water with time. The scaling of the time-axis is different for three different subsections of time series (USTS, STS and LTS).

A comprehensive laboratory study on the immersion freezing behavior of illite NX particles

N. Hiranuma et al.

Title Page

Abstract	Introduction
Conclusions	References
Tables	Figures

|◄ | ►|

◄ | ►

Back | Close

Full Screen / Esc

Printer-friendly Version

Interactive Discussion

Title Page

Abstract | Introduction

Conclusions | References

Tables | Figures

|◄ | ►|

◄ | ►

Back | Close

Full Screen / Esc

Printer-friendly Version

Interactive Discussion

Figure 4. Inter-comparison of seventeen instruments with $n_{s,BET}$. Black and red lines are interpolated lines used for T-binned averaging. Note that M-AL and M-AT results are presented in **(d)**. In **(k)**, the interpolated FRIDGE results of default (top) and imm.mode (bottom) are presented. Both ZINC (top) and IMCA-ZINC (bottom) interpolated lines are shown in **(p)**. Reference immersion freezing $n_s(T)$ spectra for illite NX (B12), K-feldspar (A13), ATD and desert dusts (Dust) (N12) are also shown (See Sect. 3.2).

Figure 5. Geometric size-based ice nucleating surface, $n_{s,geo}$, of seventeen measurement techniques. Note that M-AL and M-AT results are presented in **(d)**. Reference immersion freezing $n_s(T)$ spectra for illite NX (B12), K-feldspar (A13), ATD and desert dusts (Dust) (N12) are also shown (See Sect. 3.2).
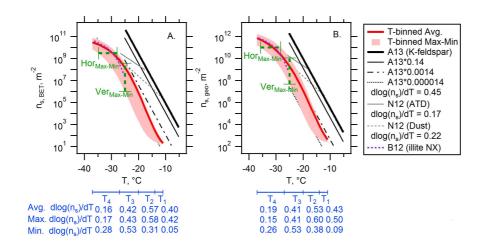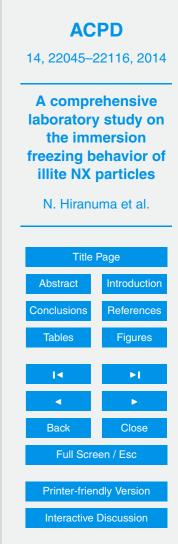
Figure 6. Immersion freezing $n_s(T)$ spectra of illite NX particles from seventeen instruments calculated as function of the BET **(a)** and geometric **(b)** surface areas. Literature results are shown for ATD and desert dusts (Niemand et al., 2012), illite (Broadley et al., 2012) and K-feldspar (Atkinson et al., 2013). Dry-dispersed particle measurements **(c)** and suspension measurements **(d)** are grouped in red and blue markers, respectively, to highlight the difference between dry particle and suspension subsets.

Figure 7. The n_s parameterization, based on the BET **(a)** and geometric **(b)** surface areas, as a function of temperature (T). The multiple exponential distribution fit (also known as the Gumbel cumulative distribution function) is expressed as $n_{s,BET}(T) = \exp(23.82 \times \exp(-\exp(0.16 \times (T + 17.49))) + 1.39)$ or $n_{s,geo}(T) = \exp(25.75 \times \exp(-\exp(0.13 \times (T + 17.17))) + 3.34)$. Note that n_s and T are in m^{-2} and °C, respectively. The deviation between maxima and minima in horizontal and vertical axis corresponds to $Hor_{Max-Min}$ and $Ver_{Max-Min}$, respectively. All fit parameters shown in Table 3.
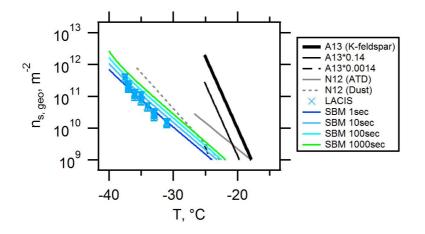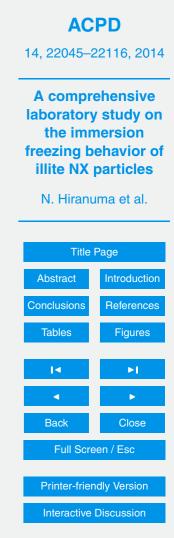
Figure 8. T-binned $n_{s,geo}$ **(a)** and $n_{s,BET}$ **(b)**. T-binned average data (i.e., 1 °C bins for 37 °C $< T < -11$ °C) of $n_s(T)$ spectra are presented for (i). All interpolated dataset (All), (ii). Suspension-measurements (Sus), (iii). Dry-dispersed particle measurements (Dry), and iv. comparison between Sus. and Dry. Red sticks represent maxima (positive direction) and minima (negative direction) and black sticks represent ± standard error. Literature results (B12, A13, and N12) are also shown.

Figure 9. Soccer ball model analysis for time-dependency of immersion freezing of illite NX particles. Comparison to LACIS measurements in $n_{s,geo}$ space is also shown. Error bars represent experimental uncertainties ($T \pm 0.3\,°C$ and $n_s \pm 28\,\%$). A shift in the residence time from 1 to 10 s shifts in n_s or n_m towards higher temperatures by about 1 °C.
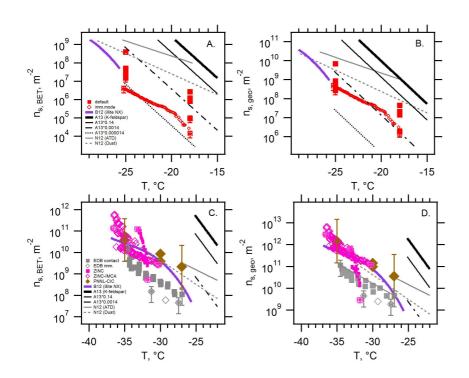
Figure 10. Examination of mode-dependency of heterogeneous ice nucleation of illite NX particles. **(a)** comparison of FRIDGE (default) to FRIDGE (imm.mode) in $n_{s,BET}$, **(b)** comparison of FRIDGE (default) to FRIDGE (imm.mode) in $n_{s,geo}$, **(c)** comparison between EDB (contact), EDB (imm.), ZINC, IMCA-ZINC and PNNL-CIC data in $n_{s,BET}$, **(d)**. comparison between EDB (contact), EDB (imm.), ZINC, IMCA-ZINC and PNNL-CIC data in $n_{s,geo}$.